New Journal of Physics

The open access journal at the forefront of physics

PAPER

CrossMark

Stochastic harmonic trapping of a Lévy walk: transport and first-passage dynamics under soft resetting strategies

Pengbo Xu[1], Tian Zhou[2], Ralf Metzler[3,*] 🕩 and Weihua Deng[2,*] 🕩

[1] School of Mathematical Sciences, Peking University, Beijing 100871, People's Republic of China
[2] School of Mathematics and Statistics, Gansu Key Laboratory of Applied Mathematics and Complex Systems, Lanzhou University, Lanzhou 730000, People's Republic of China
[3] Institute of Physics & Astronomy, University of Potsdam, 14476 Potsdam, Germany
[*] Authors to whom any correspondence should be addressed.

E-mail: xupengbo@math.pku.edu.cn, zhout19@lzu.edu.cn, rmetzler@uni-potsdam.de and dengwh@lzu.edu.cn

Abstract

We introduce and study a Lévy walk (LW) model of particle spreading with a finite propagation speed combined with *soft resets*, stochastically occurring periods in which an harmonic external potential is switched on and forces the particle towards a specific position. Soft resets avoid instantaneous relocation of particles that in certain physical settings may be considered unphysical. Moreover, soft resets do not have a specific resetting point but lead the particle towards a resetting point by a restoring Hookean force. Depending on the exact choice for the LW waiting time density and the probability density of the periods when the harmonic potential is switched on, we demonstrate a rich emerging response behaviour including ballistic motion and superdiffusion. When the confinement periods of the soft-reset events are dominant, we observe a particle localisation with an associated non-equilibrium steady state. In this case the stationary particle probability density function turns out to acquire multimodal states. Our derivations are based on Markov chain ideas and LWs with multiple internal states, an approach that may be useful and flexible for the investigation of other generalised random walks with soft and hard resets. The spreading efficiency of soft-rest LWs is characterised by the first-passage time statistic.

1. Introduction

Lévy flights (LFs), jump processes whose jump lengths ℓ follow a Lévy stable law with power-law asymptote $\simeq |\ell|^{-1-\alpha}$ ($0 < \alpha < 2$), were coined by Mandelbrot [1], who, inter alia, used them to account for empirically observed fat-tailed distributions of speculative prices on financial markets [2]. While LFs may occur naturally along the contour of long and sufficiently quickly relaxing polymer and DNA chains through hopping across loops [3, 4], generally jump processes with very long, instantaneous relocation events of massive particles appear physically problematic. To remedy this fact Lévy walks (LWs) with a *finite* propagation speed were introduced [5]. In particular, the resulting coupling of jump lengths and walk times effects finite moments of all orders for LWs as compared to the infinite variance of LFs [5].

LFs and LWs have been widely advocated as efficient search processes in one and two dimensions due to the occurrence of occasional long relocations, that reduce local oversampling in comparison to a Brownian walk [6–10]. In movement ecology, the LF foraging hypothesis [11] has become one of the ground hypotheses for optimised random search for sparse food sources. While more recently it has been pointed out that LFs and LWs may not always minimise search times and/or target localisation probabilities [12–14] they represent widely identified patterns in movement ecology [15, 16].

LW statistics were shown to characterise human hunter-gatherer foraging [17], pedestrian movement [18], human movement patterns [19] as well as COVID-19 pandemic propagation [20], and they were shown to emerge in optimised robotic search [21]. More microscopically, LWs were observed for the

motion of individual molecular motors in living biological cells [22] and for the motor-driven transport of single messenger RNA molecules in live dendritic cells [23]. We also mention LW statistics in the spreading of cancer cells [24] as well as in human memory retrieval [25] and cognition processes [26].

In physical settings LWs have been very successfully used to describe the dynamics of particles in weakly chaotic systems, in which motion events in phase space are interspersed by sticking events, e.g. around stable islands or in eddies [27–30]. LWs also describe the blinking dynamics of quantum dots [31], and they may emerge from deterministic nonlinear systems near a critical point [32]. More information about LWs can be found in the detailed recent review [33].

Another stochastic mechanism to improve the search efficiency of random search processes in many scenarios is stochastic resetting (SR) [34–36]: a diffusing particle is occasionally (at fixed time intervals or stochastically) 'reset' to a specified location. In most settings SR leads to a non-equilibrium steady state (NESS) characterised by a large deviation function [34, 37]. Generically, if the target location is within the typical range explored by the reset trajectory the search process becomes more efficient. SR has also been extended to numerous non-Markovian and non-Gaussian scenarios, including long-ranged correlated processes [38] and geometric Brownian motion [39]. Typical applications include molecular chemical reactions with stochastic decay [40], backtracking RNA polymerase scenarios [41], enzymatic reactions [42, 43], pollination strategies [44], or web search algorithms [45, 46], inter alia. Another recent generalisation is SR with random amplitudes as effective models for systems experiencing occasional crises such as riverbed sedimentation, population dynamics, and financial markets [47].

One objection against such resetting mechanisms is that, similar to the long instantaneous jumps for LFs, sudden relocation events during resets that are long compared to the diffusive distance covered by the undisturbed particle, may not be considered physical. In LFs this problem was mended by introducing a spatiotemporal coupling and thus a finite propagation speed. For resetting we here introduce *soft resets*, considering the dynamical response of the particle to an harmonic external potential that is switched on an off stochastically. In fact the experimental SR of colloidal particles in a switching optical tweezers trap recently demonstrated in [48] is a direct example for soft resetting, especially for relatively shallow trap stiffness, as optical tweezers exert a Hookean force on the trapped dielectric particle. We here combine the soft resetting procedure with LW dynamics and obtain a rich and versatile model for the description of physically regularised spreading and search processes of particles with finite propagation speed.

Direct applications of this model include the movement of animals who venture out and occasionally return towards the central area of their territory, but not always to the same nest. Similarly, these could be young animals who are called back by the parental group when they stray away too far, and when it is sufficient that they return to within the field of vision. In financial markets soft resets may serve as models for monetary interventions by central banks, attempting to curb excessive market developments. On a more microscopic scale, soft-reset LWs may represent molecular motors that are influenced by shallow optical tweezers that are switched stochastically. Such tweezers could also be combined with colloidal tracers in weakly chaotic fluids. In both cases such a setup would also allow for experimental probing the response behaviour of particles in non-equilibrium systems.

In what follows we develop and analyse the LW model with soft stochastic resets. In section 2 we construct the mathematical framework, followed by the exploration of the statistical properties for various combinations of the laws for the waiting times in the LW and the resetting times in section 3. In particular, we demonstrate the emergence of multimodal stationary probability density functions (PDFs) in the NESS of the reset process. The spreading dynamics of soft-rest LWs is analysed in section 4 in terms of the first-passage time PDF and the mean first-passage time. We discuss our results and draw our conclusions in section 5. Finally, in the appendices we collect some more formal calculations.

2. Model

We develop the soft-rest LW model in one dimension. It consists of two distinct phases, the free LW motion phase and the non-instantaneous soft-resetting phase. In the first phase we assume that the particle moves symmetrically with the constant speed v_0, so that the LW velocity can be $\pm v_0$, with probability of $1/2$ for going left or right ($-$ or $+$). The duration (waiting) time τ for each LW motion event is taken to be an independent identically distributed (i.i.d.) random variable whose PDF is denoted by $\phi^{(1)}(\tau)$. In this ordinary LW phase, if the particle just finishes one step of the walk and arrives at position x at time t, then it left either $x - v_0\tau$ or $x + v_0\tau$ at time $t - \tau$, each with probability $1/2$ [33]. In the soft-resetting phase the particle is driven by the harmonic potential $V(x) = \frac{\gamma}{2}x^2$, giving rise to the restoring Hookean force $F(x) = -\gamma x$ directed to the origin with the force constant γ. If the harmonic external potential stems from a stochastically switched optical tweezer, γ corresponds to the (adjustable) tweezer trap stiffness.

In a constantly acting harmonic potential the LW is trapped [49]. When the harmonic potential is switched on at a given location of this phase at position z and the trapping is parameterised by the time variable η, the position x of a particle with mass m satisfies the set of equations [49]

$$
\begin{cases}
m\dfrac{\mathrm{d}^2 x}{\mathrm{d}\eta^2} = -\gamma x \\[2mm]
\dfrac{\mathrm{d}x}{\mathrm{d}\eta}\bigg|_{\eta=0} = \pm v_0,
\end{cases} \tag{1}
$$

where the second equation represents the fact that the initial velocity for each soft-rest phase is v_0 or $-v_0$. In this paper we consider the symmetric case so that the probability for each case is $1/2$. From the initial position z we can then write down the solution to the ordinary differential equations (1) in the form

$$
x = z \cos(\omega\eta) \pm \frac{v_0}{\omega} \sin(\omega\eta) \tag{2}
$$

with $\omega = \sqrt{\gamma/m}$. In our approach here we consider η to be an i.i.d. random variable following the PDF $\phi^{(2)}(\eta)$. An alternative formulation could include a damping term for the motion in the harmonic potential. This scenario, of particular relevance when ω is large, will be considered elsewhere.

Now we can treat these two phases as two internal states introduced in the Markov chain approach in [50, 51], and we construct a 2×2 transition matrix M, that we assume to have the form
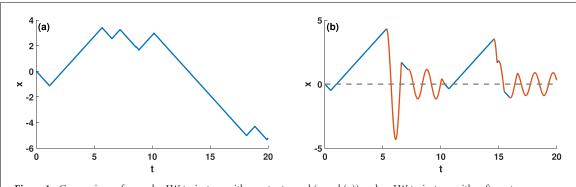
$$
M = \begin{pmatrix} M_{11} & M_{12} \\ M_{21} & M_{22} \end{pmatrix}, \tag{3}
$$

where $M_{ij} \geq 0$ $(i,j = 1,2)$ represents the probability of transitioning from state i to j. Moreover we assume that the sums of each row equal unity, i.e. $(1,1)M^{\mathrm{T}} = (1,1)$. Additionally we denote the initial distribution for the internal states as $\boldsymbol{\xi} = (\xi^{(1)}, \xi^{(2)})^{\mathrm{T}}$ with $\xi^{(1)}, \xi^{(2)} \geq 0$ and $\xi^{(1)} + \xi^{(2)} = 1$. In this vein, in the following the superscript with a bracket represents the corresponding state, e.g. $x^{(i)}$ denotes the particle arrives at location x in state i. Then the LW process under stochastic harmonic trapping can be illustrated as follows: when the particle starts to move at the initial position x_0, it will stochastically choose to stay in phase one (or two) with probability $\xi^{(1)}$ (or $\xi^{(2)} = 1 - \xi^{(1)}$), then the particle follows a free LW and moves to $x_1^{(1)} = x_0 \pm v_0\tau$ with τ generated from the PDF $\phi^{(1)}(\tau)$. Alternatively the particle starts the second phase and moves to $x_1^{(2)} = x_0 \cos(\omega\eta) \pm v_0/\omega \sin(\omega\eta)$, where η is chosen from the law $\phi^{(2)}(\eta)$. When process has just finished its Nth motion event $(N \geq 1)$ and arrives at $x_N^{(i)}$ with $i = 1,2$, then for the $(N+1)$th step, we have the possible outcomes

$$
\begin{cases}
x_{N+1}^{(1)} = x_N^{(i)} + v_0\tau, & \text{with probability } \dfrac{M_{i1}}{2}; \\[3mm]
x_{N+1}^{(1)} = x_N^{(i)} - v_0\tau, & \text{with probability } \dfrac{M_{i1}}{2}; \\[3mm]
x_{N+1}^{(2)} = x_N^{(i)} \cos(\omega\eta) + \dfrac{v_0}{\omega} \sin(\omega\eta), & \text{with probability } \dfrac{M_{i2}}{2}; \\[3mm]
x_{N+1}^{(2)} = x_N^{(i)} \cos(\omega\eta) - \dfrac{v_0}{\omega} \sin(\omega\eta), & \text{with probability } \dfrac{M_{i2}}{2},
\end{cases} \tag{4}
$$

where τ and η are random variables with respect to the PDFs $\phi^{(1)}(\tau)$ and $\phi^{(2)}(\eta)$. From the particle dynamics we can thus express how the harmonic potential stochastically acts on the LW particle via the transition matrix M. It should be noted that the first two relations in equation (4) describe the free LW process, which may be referred to as the 'walking' phase in the blue lines of figure 1(b). Conversely, the third and last relations in equation (4) describe the effect of the harmonic potential, which may be referred to as the 'soft-reset' phase related to the red curves of figure 1(b).

In figure 1 we show a comparison between a standard trajectory of a free, undisturbed LW with power-law travel time PDF (40) with $\alpha = 1.5$ (panel (a)), and a soft-reset LW with exponential resetting time PDF (panel (b)). We note the characteristic difference of soft-reset events to hard resets: while the latter would have an infinite slope and instantaneously reset the particle to its origin, the soft-reset dynamics represented by the red lines in panel (b) exhibit non-linear relaxation dynamics in the harmonic potential. Moreover, the relaxation typically does not reset the particle to its origin. Instead, the particle either leaves the soft-reset phase before reaching the origin, or it may overshoot the origin in partial oscillations in the harmonic potential. In an extended scenario (not considered here), one might also include damping in the soft-reset phase. Measured trajectories $x(t)$ may thus provide vital clues towards the

Figure 1. Comparison of a regular LW trajectory with constant speed (panel (a)) and an LW trajectory with soft resets (panel (b)). In (b) the initial distribution of states is $\boldsymbol{\xi} = (1/2, 1/2)^{\mathrm{T}}$ and $M_{i,j} = 1/2$, and the PDF $\phi^{(2)}(\tau)$ for the soft reset times is exponential with unit characteristic time. In both panels the blue lines represent the free 'walking' phase (i.e. the first state of an undisturbed LW) described by the first two relations in equation (4), and the red line corresponds to the 'soft-reset' phase (i.e. the second state) described by the third and last relations in equation (4). In both panels $v_0 = 1$ and the PDF $\phi^{(1)}(\tau)$ of relocation times in the free LW phase has the power-law form (40) with $\alpha = 1.5$. In (b) we chose $\omega = 4$.

reset-time PDF as well as how well the harmonic model chosen here for the soft-reset driving describes the observed dynamics.

Next we derive the equation for the PDF $p(x, t)$ of finding the particle at position x at time t. In the following we denote $S_t \in \{1, 2\}$ as the internal state in which the particle is encountered at a given time t, and the joint probability of S_t and the position of the particle at time t is denoted as $p^{(i)}(x, t) = p(x, S_t = i, t)$ with $i = 1, 2$. Obviously these quantities fulfil the relation

$$p(x, t) = p^{(1)}(x, t) + p^{(2)}(x, t). \tag{5}$$

From LW theory [33] and the formulation of stochastic processes with internal states [50, 51], $p^{(i)}(x, t)$ can be expressed by help of the PDFs $q^{(1,2)}(x', t')$, which state that the renewal event finishes at time t' and the particle arrives at position x' with state 1 or 2. For brevity we will drop the primes in the following. Then, according to the probabilistic statements in equation (4), the equations for $q^{(1,2)}(x, t)$ follow in the form

$$\begin{pmatrix} q^{(1)}(x, t) \\ q^{(2)}(x, t) \end{pmatrix} = \int_{-\infty}^{\infty} \mathrm{d}y \int_0^t \mathrm{d}\tau M^{\mathrm{T}} \begin{pmatrix} \nu^{(1)}(x, y, \tau) & 0 \\ 0 & \nu^{(2)}(x, y, \tau) \end{pmatrix} \begin{pmatrix} \phi^{(1)}(\tau) & 0 \\ 0 & \phi^{(2)}(\tau) \end{pmatrix} \begin{pmatrix} q^{(1)}(y, t - \tau) \\ q^{(2)}(y, t - \tau) \end{pmatrix}$$
$$+ p_0(x)\delta(t)\boldsymbol{\xi}, \tag{6}$$

where

$$\nu^{(1)}(x, y, \tau) = \frac{1}{2}\left[\delta_{\mathrm{D}}(x - y - v_0\tau) + \delta_{\mathrm{D}}(x - y + v_0\tau)\right],$$
$$\nu^{(2)}(x, y, \tau) = \frac{1}{2}\left[\delta_{\mathrm{D}}\left(x - y\cos(\omega\tau) - \frac{v_0}{\omega}\sin(\omega\tau)\right)\delta_{\mathrm{D}}\left(x - y\cos(\omega\tau) + \frac{v_0}{\omega}\sin(\omega\tau)\right)\right], \tag{7}$$

and $\delta_{\mathrm{D}}(\cdot)$ is the Dirac δ function. Moreover, $p_0(x)$ in equation (6) represents the initial distribution of the particle position, here we choose $p_0(x) = \delta_{\mathrm{D}}(x - x_0)$. Finally we have

$$\begin{pmatrix} p^{(1)}(x, t) \\ p^{(2)}(x, t) \end{pmatrix} = \int_{-\infty}^{\infty} \mathrm{d}y \int_0^t \mathrm{d}\tau M^{\mathrm{T}} \begin{pmatrix} \nu^{(1)}(x, y, \tau)\Psi^{(1)}(\tau) \\ \nu^{(2)}(x, y, \tau)\Psi^{(2)}(\tau) \end{pmatrix} \begin{pmatrix} q^{(1)}(y, t - \tau) \\ q^{(2)}(y, t - \tau) \end{pmatrix}, \tag{8}$$

where $\Psi^{(i)}(\tau) = \int_\tau^\infty \phi^{(i)}(r)\mathrm{d}r$ represents the survival probability. The Laplace transform

$$\hat{g}(s) = \mathscr{L}_t\{g(t)\}(s) = \int_0^\infty \mathrm{e}^{-st}g(t)\mathrm{d}t \tag{9}$$

of $\Psi^{(i)}(\tau)$ with respect to τ is $\widehat{\Psi}^{(i)}(s) = \frac{1}{s}(1 - \hat{\phi}^{(i)}(s))$. In the following, we will obtain the form of $p(x, t)$ from (5), (8) and (6) with the help of orthogonal Hermite polynomials, and choose some representative PDFs $\phi^{(1)}$ and $\phi^{(2)}$ to calculate the corresponding asymptotic behaviours of the mean squared displacement (MSD). In some cases we resort to numerical simulations.

3. Statistical properties

We first express the terms $q^{(1,2)}(x,t)$ and $p^{(1,2)}(x,t)$ from relations (6) and (8) in the form of Hermite orthogonal polynomials, as introduced in appendix A. The asymptotic behaviours of the MSDs with different transition matrices M and different types of the laws $\phi^{(1)}(\tau)$ and $\phi^{(2)}(\tau)$ will be calculated.

It can be obtained from equation (6) that

$$
\begin{aligned}
q^{(1)}(x,t) - \xi^{(1)}\delta_{\mathrm{D}}(x-x_0)\delta_{\mathrm{D}}(t) = {} & \frac{M_{11}}{2}\int_0^t q^{(1)}(x+v_0\tau, t-\tau)\phi^{(1)}(\tau)\mathrm{d}\tau \\
& + \frac{M_{11}}{2}\int_0^t q^{(1)}(x-v_0\tau, t-\tau)\phi^{(1)}(\tau)\mathrm{d}\tau \\
& + \frac{M_{21}}{2}\int_0^t q^{(2)}(x+v_0\tau, t-\tau)\phi^{(1)}(\tau)\mathrm{d}\tau \\
& + \frac{M_{21}}{2}\int_0^t q^{(2)}(x-v_0\tau, t-\tau)\phi^{(1)}(\tau)\mathrm{d}\tau,
\end{aligned}
\tag{10}
$$

and

$$
\begin{aligned}
q^{(2)}(x,t) - \xi_2\delta_{\mathrm{D}}(x-x_0)\delta_{\mathrm{D}}(t) = {} & \frac{M_{12}}{2}\int_0^t \left[q^{(1)}(x_+, t-\tau) + q^{(1)}(x_-, t-\tau)\right]\frac{\phi^{(2)}(\tau)}{|\cos(\omega\tau)|}\,\mathrm{d}\tau \\
& + \frac{M_{22}}{2}\int_0^t \left[q^{(2)}(x_+, t-\tau) + q^{(2)}(x_-, t-\tau)\right]\frac{\phi^{(2)}(\tau)}{|\cos(\omega\tau)|}\,\mathrm{d}\tau,
\end{aligned}
\tag{11}
$$

where $x_\pm = x/\cos(\omega\tau) \pm (v_0/\omega)\tan(\omega\tau)$. In the following we assume that $q^{(i)}(x,t)$ can be explicitly expressed by Hermite polynomials $H_n(x)$, see (A2). Specifically,

$$
q^{(i)}(x,t) = \sum_{n=0}^{\infty} H_n(x)\mathrm{e}^{-x^2} T_n^{(i)}(t), \quad \text{for } i = 1,2,
\tag{12}
$$

where the temporal terms $T_n^{(i)}(t)$ remain to be determined. Following the derivations in appendix B, we have the following recursion relations

$$
\begin{aligned}
\sqrt{\pi}2^n n! T_n^{(1)}(t) - \xi^{(1)}\delta_{\mathrm{D}}(t)H_n(x_0) = {} & \frac{\sqrt{\pi}}{2}\sum_{k=0}^n \frac{n!}{(n-k)!}\left(1+(-1)^{n-k}\right)2^n v_0^{n-k}\int_0^t \tau^{n-k}\phi^{(1)}(\tau) \\
& \times \left(M_{11}T_k^{(1)}(t-\tau) + M_{21}T_k^{(2)}(t-\tau)\right)\mathrm{d}\tau
\end{aligned}
\tag{13}
$$

and

$$
\begin{aligned}
\sqrt{\pi}2^n n! T_n^{(2)}(t) - H_n(x_0)\xi_2\delta_{\mathrm{D}}(t) = {} & \frac{\sqrt{\pi}}{2}\sum_{k=0}^n\sum_{j=0}^{\lfloor\frac{k}{2}\rfloor}\frac{2^{n-2j}n!}{j!(n-k)!}\left((-1)^j + (-1)^{n-k+j}\right)\left(\frac{v_0}{\omega}\right)^{n-k} \\
& \times \int_0^t \cos^{k-2j}(\omega\tau)\sin^{2j+n-k}(\omega\tau)\phi^{(2)}(\tau) \\
& \times \left(M_{12}T_{k-2j}^{(1)}(t-\tau) + M_{22}T_{k-2j}^{(2)}(t-\tau)\right)\mathrm{d}\tau.
\end{aligned}
\tag{14}
$$

Following a Laplace transformation with respect to time t in equations (13) and (14) we obtain the following solvable equations

$$
\begin{aligned}
\sqrt{\pi}2^n n! \widehat{T}_n^{(1)}(s) - \xi^{(1)}H_n(x_0) = {} & \frac{\sqrt{\pi}}{2}\sum_{k=0}^n\frac{n!}{(n-k)!}\left(1+(-1)^{n-k}\right)2^n v_0^{n-k}\frac{\mathrm{d}^{n-k}}{\mathrm{d}s^{n-k}}\hat{\phi}^{(1)}(s) \\
& \times \left(M_{11}\widehat{T}_k^{(1)}(s) + M_{21}\widehat{T}_k^{(2)}(s)\right),
\end{aligned}
\tag{15}
$$

and

$$\sqrt{\pi} 2^n n! \widehat{T}_n^{(2)}(s) - H_n(x_0)\xi_2 = \frac{\sqrt{\pi}}{2} \sum_{k=0}^{n} \sum_{j=0}^{\lfloor \frac{k}{2} \rfloor} \frac{2^{n-2j} n!}{j!(n-k)!} \left((-1)^j + (-1)^{n-k+j} \right) \left(\frac{v_0}{\omega} \right)^{n-k}$$
$$\times \mathscr{L}_\tau \left\{ \cos^{k-2j}(\omega\tau) \sin^{2j+n-k}(\omega\tau) \phi^{(2)}(\tau) \right\}(s) \left(M_{12} \widehat{T}_{k-2j}^{(1)}(s) + M_{22} \widehat{T}_{k-2j}^{(2)}(s) \right),$$

(16)

where $\mathscr{L}_\tau\{\cdot\}(s)$ represents the Laplace transform with respect to τ and introducing the Laplace variable s, as defined in (9). In analogy to equation (12) we also express

$$p^{(i)}(x,t) = \sum_{n=0}^{\infty} H_n(x) e^{-x^2} R_n^{(i)}(t), \quad \text{for } i = 1, 2,$$

(17)

where the terms $R_n^{(i)}(t)$ are to be determined. Through relation (8) and with similar derivations in appendix B, for each $n = 0, 1, \ldots$ we have the following recursion equations in Laplace space,

$$\widehat{R}_n^{(1)}(s) = \sum_{k=0}^{n} \frac{v_0^{n-k}}{2(n-k)!} \left(1 + (-1)^{n-k} \right) \frac{d^{n-k}}{ds^{n-k}} \widehat{\Psi}^{(1)}(s) \left(M_{11} \widehat{T}_k^{(1)}(s) + M_{21} \widehat{T}_k^{(2)}(s) \right)$$

(18)

and

$$\widehat{R}_n^{(2)}(s) = \sum_{k=0}^{n} \sum_{j=0}^{\lfloor \frac{k}{2} \rfloor} \frac{2^{-2j-1}}{j!(n-k)!} \left((-1)^j + (-1)^{n-k+j} \right)$$
$$\times \left(\frac{v_0}{\omega} \right)^{n-k} \mathscr{L}_\tau \left\{ \cos^{k-2j}(\omega\tau) \sin^{2j+n-k}(\omega\tau) \Psi^{(2)}(\tau) \right\}(s) \left(M_{12} \widehat{T}_{k-2j}^{(1)}(s) + M_{22} \widehat{T}_{k-2j}^{(2)}(s) \right).$$

(19)

Let us first verify the normalisation of $p(x,t)$, i.e. $\int_{-\infty}^{\infty} p(x,t) dx = 1$. With the definition of the Fourier transform, $\tilde{f}(k) = \mathscr{F}_x\{f(x)\}(k) = \int_{-\infty}^{\infty} e^{-ikx} f(x) dx$, the normalisation can be equivalently verified in Fourier–Laplace space by $\hat{\tilde{p}}(k,s)|_{k=0} = 1/s$. Then, from the assumed form (17) and the property (A6) of the Hermite polynomials, we see that

$$\hat{\tilde{p}}(k,s) = \hat{\tilde{p}}^{(1)}(k,s) + \hat{\tilde{p}}^{(2)}(k,s) = \sum_{n=0}^{\infty} \sqrt{\pi}(-ik)^n \exp\left(-\frac{k^2}{4} \right) \left(R_n^{(1)}(s) + R_n^{(2)}(s) \right).$$

(20)

Then with $k = 0$ we find

$$\hat{\tilde{p}}(k,s) \Big|_{k=0} = \sqrt{\pi} \left(R_0^{(1)}(s) + R_0^{(2)}(s) \right).$$

(21)

From relations (18) and (19) we have

$$\widehat{R}_0^{(i)}(s) = \widehat{\Psi}^{(i)}(s) \left(M_{1i} \widehat{T}_0^{(1)}(s) + M_{2i} \widehat{T}_0^{(2)}(s) \right),$$

(22)

and with the recursion relations (15) and (16),

$$\begin{cases} \widehat{T}_0^{(1)}(s) - \dfrac{\xi^{(1)}}{\sqrt{\pi}} = \hat{\phi}^{(1)}(s) \left(M_{11} \widehat{T}_0^{(1)}(s) + M_{21} \widehat{T}_0^{(2)}(s) \right) \\[2mm] \widehat{T}_0^{(2)}(s) - \dfrac{\xi_2}{\sqrt{\pi}} = \hat{\phi}^{(2)}(s) \left(M_{12} \widehat{T}_0^{(1)}(s) + M_{22} \widehat{T}_0^{(2)}(s) \right), \end{cases}$$

(23)

where we note that $H_0(x) = 1$, see also equation (A2). Then by solving equation (23) and substituting into relation (22) we verify that

$$\widehat{R}_0^{(1)}(s) + \widehat{R}_0^{(2)}(s) = \frac{1}{\sqrt{\pi} s},$$

(24)

where the relations $M_{12} = 1 - M_{11}$, $M_{21} = 1 - M_{12}$ and $\xi^{(1)} = 1 - \xi^{(2)}$ are used during the calculations. Then from result (24) the normalisation follows, see equation (21).

To obtain the time dependence of the MSD we use the relation for the *m*th moment of the PDF $p(x,t)$ in Fourier space,

$$\langle x^m(t) \rangle = i^m \frac{d^m}{dk^m} \tilde{p}(k,t) \bigg|_{k=0}. \tag{25}$$

Using equation (20) we find that

$$\begin{aligned}
\langle \hat{x}^2(s) \rangle &= \mathscr{L}_t \left\{ \langle x^2(t) \rangle \right\}(s) \\
&= \frac{\sqrt{\pi}}{2} \left(\widehat{R}_0^{(1)}(s) + \widehat{R}_0^{(2)}(s) \right) + 2\sqrt{\pi} \left(\widehat{R}_2^{(1)}(s) + \widehat{R}_2^{(2)}(s) \right) \\
&= \frac{1}{2s} + 2\sqrt{\pi} \left(\widehat{R}_2^{(1)}(s) + \widehat{R}_2^{(2)}(s) \right),
\end{aligned} \tag{26}$$

where the last equation utilises relation (24). Therefore, in order to calculate the asymptotic behaviour of the MSD, we need to obtain the results of $\widehat{R}_0^{(1,2)}(s)$ and $\widehat{R}_2^{(1,2)}(s)$ through equations (18) and (19). Moreover, $\widehat{T}_0^{(1,2)}$ and $\widehat{T}_2^{(1,2)}$ given by expressions (15) and (16) are required to calculate $\widehat{R}_0^{(1,2)}(s)$ and $\widehat{R}_2^{(1,2)}(s)$. It should be noted that, if we choose the initial position to be the origin, $x_0 = 0$, then from relation (25) the Laplace transform of the mean value reads

$$\langle \hat{x}(s) \rangle = \sqrt{\pi} \left(\widehat{R}_1^{(1)}(s) + \widehat{R}_1^{(2)}(s) \right). \tag{27}$$

Then from equations (18) and (19) we obtain

$$\begin{aligned}
\widehat{R}_1^{(1)}(s) &= \widehat{\Psi}^{(1)}(s) \left(M_{11} \widehat{T}_1^{(1)}(s) + M_{21} \widehat{T}_1^{(2)}(s) \right), \\
\widehat{R}_1^{(2)}(s) &= \mathscr{L}_\tau \left\{ \cos(\omega\tau) \Psi^{(2)}(\tau) \right\}(s) \left(M_{12} \widehat{T}_1^{(1)}(s) + M_{22} \widehat{T}_1^{(2)}(s) \right),
\end{aligned} \tag{28}$$

and further from equations (15) and (16),

$$\begin{aligned}
\widehat{T}_1^{(1)}(s) &= \phi^{(1)}(s) \left(M_{11} \widehat{T}_1^{(1)}(s) + M_{21} \widehat{T}_1^{(2)}(s) \right) \\
\widehat{T}_1^{(2)}(s) &= \mathscr{L}_\tau \left\{ \cos(\omega\tau) \phi^{(2)}(\tau) \right\}(s) \left(M_{12} \widehat{T}_1^{(1)}(s) + M_{22} \widehat{T}_1^{(2)}(s) \right).
\end{aligned} \tag{29}$$

Here we can see that the first moment vanishes when t is sufficiently large for the different pairs of the densities $\phi^{(1)}(t)$ and $\phi^{(2)}(t)$ examined later in this section. This fact indicates that the process is indeed (asymptotically) symmetrical.

Another quantity of interest is the kurtosis defined as

$$K = \frac{\langle x^4(t) \rangle}{\langle x^2(t) \rangle^2}, \tag{30}$$

that will be used to characterise the tails of the stationary PDF. Owing to the fact that non-Gaussian PDFs are not fully characterised by the second moment, the fourth moment can be used to examine the non-Gaussianity of a PDF. In one dimension, the value of the kurtosis for a Gaussian is $K = 3$, and deviations to smaller or larger K values, respectively, point at more concentrated and longer tailed PDFs as compared to a Gaussian. To demonstrate the non-Gaussianity of our solutions in what follows, we evaluate the kurtosis based on equations (25) and (20), from which we find the fourth moment as

$$\langle x^4(t) \rangle = \frac{3\sqrt{\pi}}{4} \left(R_0^{(1)}(t) + R_0^{(2)}(t) \right) + 6\sqrt{\pi} \left(R_2^{(1)}(t) + R_2^{(2)}(t) \right) + 24\sqrt{\pi} \left(R_4^{(1)}(t) + R_4^{(2)}(t) \right). \tag{31}$$

We denote $\langle \hat{x}^4(s) \rangle = \mathscr{L}_t \left\{ \langle x^4(t) \rangle \right\}(s)$.

To obtain concrete expressions for these quantities we consider several relevant combinations of the laws $\phi^{(2)}(\tau)$ and $\phi^{(1)}(\tau)$, the results for the MSDs are then summarised in tables 1 and 2.

3.1. The PDF $\phi^{(2)}(\tau)$ is an exponential distribution

We start with an exponential form $\phi^{(2)}(\tau) = \lambda_2 e^{-\lambda_2 \tau}$ with the characteristic time $1/\lambda_2$ for the trapping period in the harmonic soft-reset potential, in combination with different choices for the LW waiting time PDF $\phi^{(1)}(\tau)$. For each case we calculate the corresponding asymptotic behaviours of the averages and the MSDs.

Table 1. Long time behaviour of the MSD of the soft-reset LW for an exponential PDF $\phi^{(2)}$ of the trapping periods. The respective equation numbers are listed. The symbol $\simeq$ indicates asymptotic scaling without prefactors.

$\phi^{(2)}(\tau)$	$\phi^{(1)}(\tau)$	M_{11} and M_{22}	MSD $\langle x^2(t)\rangle$
$\lambda_2\,e^{-\lambda_2\tau}$	$\lambda_1\,e^{-\lambda_1\tau}$	$0\leqslant M_{11}, M_{22} < 1$	$\simeq t^0$ (32)
		$M_{11}=1, 0\leqslant M_{22}<1$	$\simeq t$ (37)
		$0\leqslant M_{11}<1, M_{22}=1$	$\simeq t^0$ (38)
		$M_{11}=M_{22}=1$	$\simeq t$ (37)
	Power-law $\alpha_1\in(0,1)$	$0\leqslant M_{11}, M_{22}<1$	$\simeq t^2$ (42)
		$M_{11}=1, 0\leqslant M_{22}<1$	$\simeq t^2$ (43)
		$0\leqslant M_{11}<1, M_{22}=1$	$\simeq t^{2-\alpha_1}$ (44)
		$M_{11}=M_{22}=1$	$\simeq t^2$ (46)
	Power-law $\alpha_1\in(1,2)$	$0\leqslant M_{11}, M_{22}<1$	$\simeq t^{3-\alpha_1}$ (48)
		$M_{11}=1, 0\leqslant M_{22}<1$	$\simeq t^{3-\alpha_1}$ (50)
		$0\leqslant M_{11}<1, M_{22}=1$	$\simeq C$ (51)
		$M_{11}=M_{22}=1$	$\simeq t^{3-\alpha_1}$ (52)

Table 2. Asymptotic scaling of the MSD for soft-reset LWs when the duration of the harmonic confinement has an asymptotic power-law PDF $\phi^{(2)}(\tau)$. The symbol $\simeq$ indicates asymptotic scaling without prefactors.

$\phi^{(2)}(\tau)$	$\phi^{(1)}(\tau)$	M_{11} and M_{22}	MSD $\langle x^2(t)\rangle$
Power-law $\alpha_2\in(0,1)$	$\lambda_1\,e^{-\lambda_1\tau}$	$0\leqslant M_{11}, M_{22}<1$	$\simeq t^0$
		$M_{11}=1, 0\leqslant M_{22}<1$	$\simeq t$
		$0\leqslant M_{11}<1, M_{22}=1$	$\simeq t^0$
		$M_{11}=M_{22}=1$	$\simeq t$
	Power-law $\alpha_1\in(0,1)$	$0\leqslant M_{11}, M_{22}<1$	If $\alpha_2<\alpha_1$: $\simeq t^{2-\alpha_1+\alpha_2}$, if $\alpha_2>\alpha_1$: $\simeq t^2$
		$M_{11}=1, 0\leqslant M_{22}<1$	$\simeq t^2$
		$0\leqslant M_{11}<1, M_{22}=1$	$\simeq t^{2-\alpha_1}$
		$M_{11}=M_{22}=1$	$\simeq t^2$
	Power-law $\alpha_1\in(1,2)$	$0\leqslant M_{11}, M_{22}<1$	$\simeq t^{3-\alpha_1}$
		$M_{11}=1\ 0\leqslant M_{22}<1$	$\simeq t^{3-\alpha_1}$
		$0\leqslant M_{11}<1, M_{22}=1$	$\simeq t^{2-\alpha_1}$
		$M_{11}=M_{22}=1$	$\simeq t^{3-\alpha_1}$
Power-law $\alpha_2\in(1,2)$	$\lambda_1\,e^{-\lambda_1\tau}$	$0\leqslant M_{11}, M_{22}<1$	$\simeq t^0$
		$M_{11}=1, 0\leqslant M_{22}<1$	$\simeq t$
		$0\leqslant M_{11}<1, M_{22}=1$	$\simeq t^0$
		$M_{11}=M_{22}=1$	$\simeq t$
	Power-law $\alpha_1\in(0,1)$	$0\leqslant M_{11}, M_{22}<1$	$\simeq t^2$
		$M_{11}=1, 0\leqslant M_{22}<1$	$\simeq t^2$
		$0\leqslant M_{11}<1, M_{22}=1$	$\simeq t^{2-\alpha_1}$
		$M_{11}=M_{22}=1$	$\simeq t^2$
	Power-law $\alpha_1\in(1,2)$	$0\leqslant M_{11}, M_{22}<1$	$\simeq t^{3-\alpha_1}$
		$M_{11}=1, 0\leqslant M_{22}<1$	$\simeq t^{3-\alpha_1}$
		$0\leqslant M_{11}<1, M_{22}=1$	$\simeq t^0$
		$M_{11}=M_{22}=1$	$\simeq t^{3-\alpha_1}$

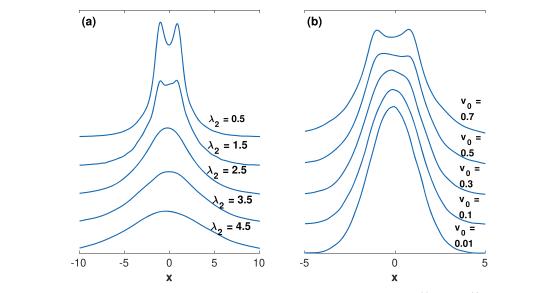### 3.1.1. The PDF $\phi^{(1)}(\tau)$ is an exponential distribution

First we consider the exponential waiting time PDF $\phi^{(1)}(\tau) = \lambda_1\,e^{-\lambda_1\tau}$ with characteristic time $1/\lambda_1$. Then from relation (27) it can be found that the average $\langle x(t)\rangle \simeq 0$ at sufficiently long times t. In the following we focus on the asymptotic behaviour of the MSD $\langle x^2(t)\rangle$ that corresponds to small values of s in Laplace space. Then from equation (26) the asymptotic behaviour of the MSD in Laplace space can be calculated by neglecting higher order terms.

(a) *The case $0\leqslant M_{11}, M_{22}< 1$.* When M_{11} and M_{22} are strictly less than one, i.e. $0\leqslant M_{11}, M_{22} < 1$, we have

$$\langle x^2(t)\rangle \sim \frac{v_0^2}{\lambda_1^2(1-M_{11})}\left[\frac{1}{\omega^2}\left(\lambda_1^2(1-M_{11})+\lambda_2^2(1-M_{22})\right)+2\left(2-M_{22}-\frac{\lambda_1(1-M_{11})}{\lambda_1(1-M_{11})+\lambda_2(1-M_{22})}\right)\right],\tag{32}$$

corresponding to a t-independent plateau value, i.e. the particle is localised. Moreover, from result (32) we conclude that the initial distribution $\boldsymbol{\xi}$ has no influence on the MSD at sufficiently long times t.

For this case $0\leqslant M_{11}, M_{22} < 1$ we now consider the stationary PDF $p^{\mathrm{st}}(x) = \lim_{t\to\infty} p(x,t)$. In figure 2 we show results from stochastic simulations, demonstrating a crossover of $p^{\mathrm{st}}(x)$ from a mono-modal to a

Figure 2. Stochastic simulations of the stationary PDF $p^{st}(x)$ for exponential forms of the PDFs $\phi^{(1)}(\tau)$ and $\phi^{(2)}(\tau)$. The lines are obtained from sampling over 5×10^4 realisations with the parameters $\boldsymbol{\xi} = (0.5, 0.5)^{\mathrm{T}}$, $M_{11} = M_{22} = 0.5$. The other parameters for (a) are $\lambda_1 = 1$, $v_0 = \omega = 1$, and for (b) $\lambda_1 = \lambda_2 = 1$, and $v_0 = \omega$. In panel (a) the convergence to a Gaussian bell curve for increasing λ_2 is distinct.

bimodal shape when the inverse time scale λ_2 decreases, or when v_0, ω increase. Although λ_1, M_{11}, and M_{22} have some influence on the stationary distribution, as well, they do not change the mono-modal or bimodal character of $p^{st}(x)$.

The existence of a stationary PDF and crossovers from mono- to bimodal shapes was previously demonstrated for LWs in a constantly applied harmonic external potential [49]. For LFs, in contrast, an harmonic external potential effects a mono-modal stationary Lévy-stable PDF with the same index of stability as the driving noise [52]. Multimodal PDFs of LFs are only realised for steeper than harmonic ('superharmonic') potentials [53–56], compare also the mono-modal shapes for 'subharmonic' external potentials in [57].

We finally consider the kurtosis K of the PDF in the stationary state, given by the asymptotic behaviour of $\langle x^4(t) \rangle$. Figure 3 shows results of simulations for different parameters as functions of the inverse time scales λ_1 and λ_2. Depending on the parameter combinations the kurtosis indicates the existence of both leptokurtic ($K > 3$) and platykurtic ($K < 3$) shapes of $p_{st}(x)$. The full lines are numerical evaluations of our explicit but intricate result (C1).

Analytically, from equation (31) by solving equations (15) and (16) for $\{\widehat{T}_i^{1,2}(s)\}_{i=0,2,4}$ as well as equations (18) and (19) for $\{\widehat{R}_i^{1,2}(s)\}_{i=0,2,4}$, the asymptotic behaviour of K is obtained after inverse Laplace transformation, see equation (C1). As can be seen in figure 3(a) at small λ_1 we have $K > 3$, i.e. a leptokurtic PDF. This is consistent with the small λ_1-limit of equation (C1),

$$\lim_{\lambda_1 \to 0} K = 3 \frac{\lambda_2^4(1 - M_{22}) + 4\lambda_2^2(5 - 4M_{22})\omega^2 + 8(8 - 3M_{22})\omega^4}{(\lambda_2^2 + 10\omega^2)(\lambda_2^2(1 - M_{22}) + 2(2 - M_{22})\omega^2)}, \tag{33}$$

which indeed leads to $\lim_{\lambda_1 \to 0} K > 3$ since the numerator minus the denominator is larger than zero,
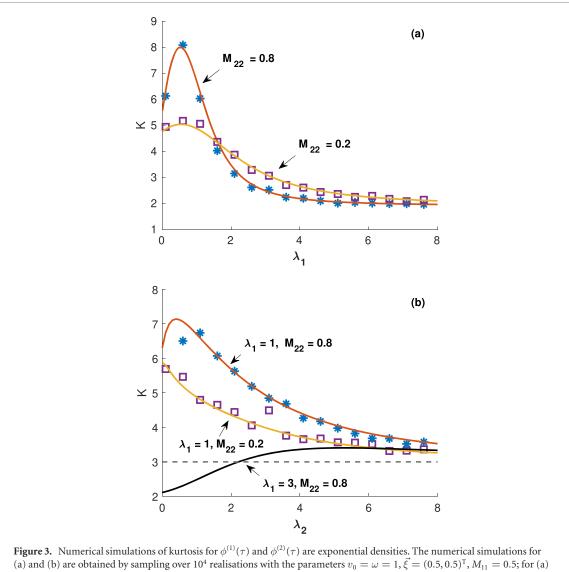
$$2\lambda_2^2(3 - 2M_{22})\omega^2 + 4(6 - M_{22})\omega^4 > 0. \tag{34}$$

Further figure 3(a) shows that $K < 3$, i.e. the PDF is platykurtic when λ_1 becomes large enough. This conclusion can also be obtained from equation (C1) by taking the limit

$$\lim_{\lambda_1 \to \infty} K = 3 \frac{\lambda_2^2 + 6\omega^2}{\lambda_2^2 + 10\omega^2} < 3. \tag{35}$$

On the other hand, we can also investigate how the kurtosis changes with λ_2. First, we take the limit of small inverse time scales λ_2, yielding

$$\lim_{\lambda_2 \to 0} K = 3\left(1 - \frac{2\lambda_1^4(1 - M_{11})^2 - 4(7 - M_{22})(1 - M_{22})\omega^4}{5(\lambda_1^4(1 - M_{11}) + 2(1 - M_{22})\omega^2)^2}\right), \tag{36}$$

Figure 3. Numerical simulations of kurtosis for $\phi^{(1)}(\tau)$ and $\phi^{(2)}(\tau)$ are exponential densities. The numerical simulations for (a) and (b) are obtained by sampling over 10^4 realisations with the parameters $v_0 = \omega = 1$, $\vec{\xi} = (0.5, 0.5)^{\mathrm{T}}$, $M_{11} = 0.5$; for (a) $\lambda_2 = 1$, the real lines are the corresponding theoretical results in (C1).

which, depending on the exact parameter values, can be smaller or larger than 3, as evidenced in figure 3(b). For all cases, interestingly, the kurtosis converges to three for large λ_2 independent of the exact parameter values, i.e. $\lim_{\lambda_2 \to \infty} K = 3$. The Gaussian PDF is indeed the expected long-time shape of an LW with exponential waiting time PDF. We conclude that for different regions of λ_1, the behaviours of kurtosis K can be different as λ_2 grows. Specifically, when $\lambda_1 < \left(\frac{2(7 - M_{22})(1 - M_{22})}{(1 - M_{11})^2} \right)^{1/4} \omega$, the kurtosis is $K > 3$ for small λ_2, indicating a leptokurtic PDF. It then changes to the Gaussian value $K = 3$ when λ_2 increases. In the other case, $\lambda_1 > \left(\frac{2(7 - M_{22})(1 - M_{22})}{(1 - M_{11})^2} \right)^{1/4} \omega$, the value of the kurtosis is $K < 3$ for small λ_2, indicating a platykurtic PDF. It then assumes $K > 3$ for intermediate λ_2, and then finally converges to the Gaussian value $K = 3$. Therefore, the behaviour of the kurtosis is completely different from the LW in a constantly switched-on harmonic external potential [49].

(b) *The case $M_{11} = 1$ and $0 \leqslant M_{22} < 1$.* When $M_{11} = 1$ and $0 \leqslant M_{22} < 1$,

$$\langle x^2(t) \rangle \sim \frac{2v_0^2}{\lambda_1} t, \tag{37}$$

i.e. the process is not confined, and the MSD growth is unbounded. Indeed, for this choice of M_{11} and M_{22} the particle simply follows the dynamics of an ordinary one-dimensional symmetric LW with constant speed v_0. Due to the exponential waiting time PDF the MSD shows the linear growth found in expression (37).

(c) *The case $M_{22} = 1$ and $0 \leqslant M_{11} < 1$.* The opposite case is given when $M_{22} = 1$ and $0 \leqslant M_{11} < 1$. This is the case of an LW, that is constantly influenced by an external harmonic potential. The result obtained here is then the same as derived in [49], namely, we find the MSD plateau

$$\langle x^2(t) \rangle \sim \frac{v_0^2}{\omega^2}. \tag{38}$$

(d) *The case $M_{11} = M_{22} = 1$.* For the last case, $M_{11} = M_{22} = 1$, the transition matrix M is the identity matrix I, and therefore we can treat this process as two isolated processes: the one is a free LW particle moving in one-dimensional space with a constant speed, the other one is an LW moving in an harmonic potential. These two process are correlated though the initial distribution $\boldsymbol{\xi}$, such that at sufficiently long times we find

$$\langle x^2(t) \rangle \sim \frac{2v_0^2 \xi^{(1)}}{\lambda_1} t, \tag{39}$$

which differs from result (37) by the factor $\xi^{(1)}$.

In summary, when both PDFs $\phi^{(1)}(\tau)$ and $\phi^{(2)}(\tau)$ are of exponential shape, with finite characteristic times, in the limit of long times we either find a linear growth in time of the MSD or a plateau value. In the non-trivial case $0 \leqslant M_{11}, M_{22} < 1$, the harmonic potential is stochastically applied on the LW particle. This stochastic soft-reset is, however, sufficient to effect an NESS with a stationary PDF. The latter can attain mono-modal and bimodal shapes, depending on the parameters. For $M_{11} = 1$ and $0 \leqslant M_{22} < 1$ we have a free LW particle, and for our case of exponentially distributed waiting times the corresponding MSD grows linearly with t, i.e. indicating normal diffusion [33]. For $M_{22} = 1$ and $0 \leqslant M_{11} < 1$ we have the confined LW in a constant external potential [49], and for $M_{11} = M_{22} = 1$ the mixing of two independent dynamics (free LW and confined LW) leads to a linear growth of the MSD with t, proportional to the probability $\xi^{(1)}$ that the particle initially is free.

The dynamics of the soft-reset LW discussed here can thus be considered as a competition between free LW diffusion and localisation by the external harmonic potential. From result (32) we conclude that the LW of free normal diffusion is confined by the stochastically switched harmonic soft-reset potential. In the case when $M_{22} = 1$ and $0 \leqslant M_{11} < 1$, the fact that $M_{11} < 1$ indicates that the process may switch from the first to the second state, i.e. from free to confined motion, while $M_{22} = 1$ indicates that, once in the confined state, the process will always stay in this second state and cannot switch back to the first one, leading to the confinement expressed by result (38). From this reasoning it may appear that the result in this case will always be recovered, independent of the exact choices of $\phi^{(1)}(\tau)$ and $\phi^{(2)}(\tau)$. However, from the following discussions, we will find some cases with the same conditions on M_{11} and M_{22}, when the MSD differs from expression (38), or when even no localisation occurs.

3.1.2. The PDF $\phi^{(1)}(\tau)$ is an asymptotic power-law PDF with divergent characteristic time

In this part, we consider $\phi^{(1)}(\tau)$ to assume the form

$$\phi^{(1)}(\tau) = \frac{\alpha_1}{\tau_0 (1 + \tau/\tau_0)^{1+\alpha_1}} \tag{40}$$

encoding the asymptotic power-law $\phi^{(1)}(\tau) \sim \alpha_1 \tau_0^{\alpha_1} / \tau^{1+\alpha_1}$. For simplicity we will choose $\tau_0 = 1$. We see that when $\alpha_1 \in (0, 1)$ the characteristic time $\langle \tau \rangle$ diverges. In the long time limit, therefore, the Laplace transform of expression (40) is given by

$$\hat{\phi}^{(1)}(s) \sim 1 - \Gamma(1 - \alpha_1) s^{\alpha_1}. \tag{41}$$

(a) *The case $0 \leqslant M_{11}, M_{22} < 1$.* First we consider the 'mixing' case $0 \leqslant M_{11}, M_{22} < 1$. Following expression (26) we calculate the asymptotic behaviour of the MSD in the long time limit,
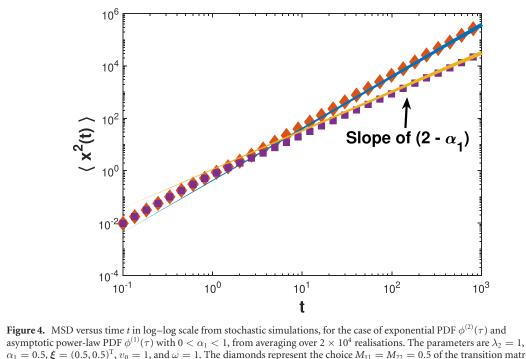
$$\langle x^2(t) \rangle \sim \frac{1}{2} (2 - \alpha_1)(1 - \alpha_1) v_0^2 t^2, \tag{42}$$

which indicates that the stochastic harmonic potential cannot localise the ballistic LW particle. Although the anomalous diffusion exponent does not change, the stochastic harmonic potential makes the LW slower, given by the factor $(2 - \alpha_1)/2$ compared with the free LW in equation (43) below, and as demonstrated in figure 4.

(b) *The case $M_{11} = 1$ and $0 \leqslant M_{22} < 1$.* For the pure LW case of $M_{11} = 1$ and $0 \leqslant M_{22} < 1$ the asymptotic behaviour of the MSD is given by

$$\langle x^2(t) \rangle \sim (1 - \alpha_1) v_0^2 t^2, \tag{43}$$

which corresponds to the result of an ordinary LW [33].

Figure 4. MSD versus time *t* in log–log scale from stochastic simulations, for the case of exponential PDF $\phi^{(2)}(\tau)$ and asymptotic power-law PDF $\phi^{(1)}(\tau)$ with $0 < \alpha_1 < 1$, from averaging over 2×10^4 realisations. The parameters are $\lambda_2 = 1$, $\alpha_1 = 0.5$, $\boldsymbol{\xi} = (0.5, 0.5)^{\mathrm{T}}$, $v_0 = 1$, and $\omega = 1$. The diamonds represent the choice $M_{11} = M_{22} = 0.5$ of the transition matrix M, and the squares correspond to the case $M_{11} = 0.5$, $M_{22} = 1$. The blue and yellow full lines which fit very well with the numerical results are the corresponding theoretical results (42) and (44), respectively.

(c) *The case $M_{22} = 1$ and $0 \leqslant M_{11} < 1$.* When $M_{22} = 1$ and $0 \leqslant M_{11} < 1$, we may intuitively expect to have the same result as in equation (38). However, instead of a localisation we obtain the following result,

$$\langle x^2(t) \rangle \sim C t^{2-\alpha_1}, \tag{44}$$

where *C* is a constant given by

$$C = \frac{2 M_{11} v_0^2 \xi^{(1)}}{1 - M_{11}}. \tag{45}$$

The behaviour in equation (44) indicates superdiffusion with anomalous scaling exponent $2 - \alpha_1$. Thus, while the soft-reset mechanism effects a reduction of the propagation from ballistic motion for the free LW and case (a) above, the diverging characteristic time of the PDF $\phi^{(1)}(\tau)$ is sufficient to counterbalance the soft-reset confinement with finite characteristic trapping period.

(d) *The case $M_{11} = M_{22} = 1$.* In the last case $M_{11} = M_{22} = 1$ the process is again divided into two independent states through the initial distribution $\boldsymbol{\xi}$. The states will not mix, such that

$$\langle x^2(t) \rangle \sim (1 - \alpha_1) \xi^{(1)} v_0^2 t^2, \tag{46}$$

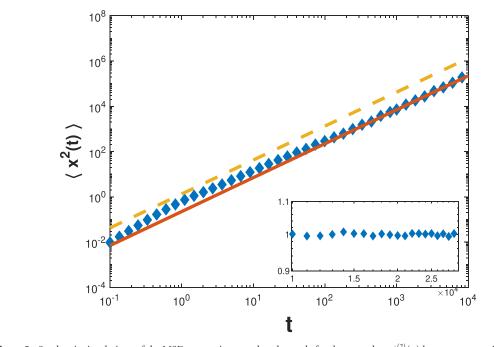i.e. we observe ballistic motion with the prefactor $\xi^{(1)}$.

3.1.3. The PDF $\phi^{(1)}(\tau)$ is an asymptotic power-law PDF with finite characteristic time but divergent second moment

We now consider the case when $\phi^{(1)}(\tau)$ is still power-law distributed as given by equation (40), but now the scaling exponent is restricted to range in the interval $1 < \alpha_1 < 2$, so that the characteristic time for the PDF $\phi^{(1)}(\tau)$ is finite, however, its second moment diverges. The Laplace transform of this $\phi^{(1)}(\tau)$ at small Laplace variable *s* corresponding to the long time limit is asymptotically given by [33]

$$\hat{\phi}^{(1)}(s) \sim 1 - \frac{1}{\alpha_1 - 1} s - \Gamma(1 - \alpha_1) s^{\alpha_1}. \tag{47}$$

(a) *The case $0 \leqslant M_{11}, M_{22} < 1$.* Following the derivation described below equation (26) the asymptotic behaviour of the MSD for the case $0 \leqslant M_{11}, M_{22} < 1$ can be obtained in the form

$$\langle x^2(t) \rangle \sim \frac{(\alpha_1 - 1)\lambda_2(1 - M_{22})v_0^2}{(3 - \alpha_1)\left[(\alpha_1 - 1)(1 - M_{11}) + \lambda_2(1 - M_{22})\right]} t^{3-\alpha_1}. \tag{48}$$

Figure 5. Stochastic simulations of the MSD versus time t on log–log scale for the case when $\phi^{(2)}(\tau)$ has an exponential shape and $\phi^{(1)}(\tau)$ is of power-law form with scaling exponent $1 < \alpha_1 < 2$. The numerical results are obtained from averaging over 2×10^4 realisations. The parameters are $\lambda_2 = 1$, $\alpha_1 = 1.5$, $\boldsymbol{\xi} = (0.5, 0.5)^{\mathrm{T}}$, $v_0 = 1$, and $\omega = 1$. The diamonds are obtained from simulations with $M_{11} = M_{22} = 0.5$, and the inset corresponds to the case $M_{11} = 0.5, M_{22} = 1$ indicating localisation. The red full line is the theoretical result (48) and the yellow dashed line above the red line represents the MSD for the free LW whose waiting time follows the same PDF $\phi^{(1)}(\tau)$.

Similar to the situation of equation (42) the soft-reset harmonic potential with finite period cannot localise the LW but effects a reduction from the ballistic to the superdiffusive behaviour with scaling exponent $3 - \alpha_1$. This result is corroborated by stochastic simulations as demonstrated in figure 5 showing nice convergence to the predicted scaling.

The PDF $p(x, t)$ for this case obtained from stochastic simulations at long times is shown in figure 6. We deduce that the asymptotic behaviour of the PDF has the power-law tail

$$p(x, t) \simeq |x|^{-\alpha_1}. \tag{49}$$

It should be noted that since LWs are spatiotemporally coupled, a particle travelling long distances is penalised by a high time cost [5, 59]. At any finite time t, a free LW with constant speed v_0 can travel a maximal distance of $\pm v_0 t$, and it is thus constrained in the interval $[-v_0 t, v_0 t]$, such that $p(x, t) = 0$ for $|x|$ outside this interval. Therefore, the long tails seen in equation (49) do not reach to infinite at any fine t, and the second moment of the LW is finite. The pre-asymptotic scaling observed in figure 6 is best fitted by the power-law $p(x, t) \simeq |x|^{-\alpha_1 + 0.4}$. This result is completely different from the case of immediate resetting with rate $0 < r < 1$ in [58], where we cannot find a crossover of the powers in the PDF but observe a single power-law with scaling exponent $-\alpha_1$.

(b) *The case $M_{11} = 1$ and $0 \leqslant M_{22} < 1$.* The simple case $M_{11} = 1$ and $0 \leqslant M_{22} < 1$ of a free LW has the ordinary LW scaling [59–62]

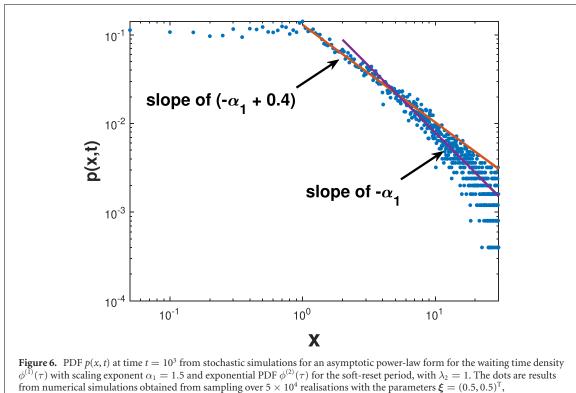$$\langle x^2(t) \rangle \sim \frac{2 v_0^2 (\alpha_1 - 1)}{(3 - \alpha_1)(2 - \alpha_1)} t^{3 - \alpha_1}. \tag{50}$$

(c) *The case $M_{22} = 1$ and $0 \leqslant M_{11} < 1$.* An interesting result of localisation in the soft-reset scenario is obtained when $M_{22} = 1$ and $0 \leqslant M_{11} < 1$. Consistent with the simulations results shown in the inset of figure 5, the MSD in the long time limit scales as

$$\langle x^2(t) \rangle \sim C, \tag{51}$$

for some constant C. This result verifies our claim that when the average of $\phi^{(1)}(\tau)$ exists, for the condition $M_{22} = 1$ and $0 \leqslant M_{11} < 1$ the harmonically soft-reset process is localised.

(d) *The case $M_{11} = M_{22} = 1$.* Finally for the independent case $M_{11} = M_{22} = 1$, the corresponding result for the MSD reads

$$\langle x^2(t) \rangle \sim \frac{2(\alpha_1 - 1)\xi^{(1)}}{(3 - \alpha_1)(2 - \alpha_1)} t^{3 - \alpha_1}, \tag{52}$$

Figure 6. PDF $p(x, t)$ at time $t = 10^3$ from stochastic simulations for an asymptotic power-law form for the waiting time density $\phi^{(1)}(\tau)$ with scaling exponent $\alpha_1 = 1.5$ and exponential PDF $\phi^{(2)}(\tau)$ for the soft-reset period, with $\lambda_2 = 1$. The dots are results from numerical simulations obtained from sampling over 5×10^4 realisations with the parameters $\boldsymbol{\xi} = (0.5, 0.5)^{\mathrm{T}}$, $M_{11} = M_{22} = 0.5$, and $v_0 = \omega = 1$.

i.e. we observe superdiffusion with coefficient $\xi^{(1)}$.

All results for the MSD of section 3.1 are summarised in table 1.

3.2. The PDF $\phi^{(2)}(\tau)$ is an asymptotic power-law

We now focus on the case when the soft-reset periods are broadly distributed according to the asymptotic power-law form

$$\phi^{(2)}(\tau) = \frac{\alpha_2}{\tau_0'(1 + \tau/\tau_0')^{1+\alpha_2}}. \tag{53}$$

We consider the two ranges $0 < \alpha_2 < 1$ and $1 < \alpha_2 < 2$ for the scaling exponent α_2, respectively corresponding to the case of diverging mean period and finite period with diverging second moment. Again we combine this PDF with different types of the LW waiting time PDF $\phi^{(1)}(\tau)$ and calculate the corresponding MSDs in the long time limit.

3.2.1. The PDF $\phi^{(1)}(\tau)$ has an exponential form

When the PDF $\phi^{(1)}(\tau)$ has an exponential distribution, we intuitively expect that the process will localise due to the asymptotically overwhelming action of the harmonic confinement. As the exact determination of the prefactors is quite complicated we only provide the resulting scaling behaviours here.

(a) *The case $0 \leqslant M_{11}, M_{22} < 1$.* In this case the LW motion with finite characteristic waiting time under the action of the soft-reset mechanism produces a localisation of the form
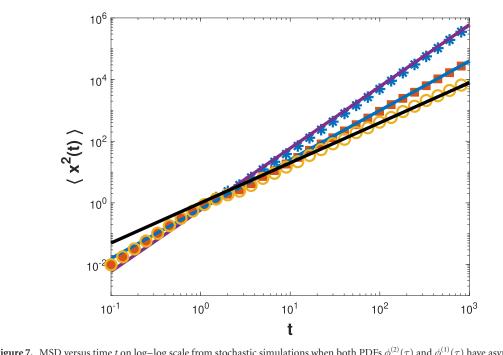
$$\langle x^2(t) \rangle \sim C_1 \tag{54}$$

for the MSD, with the constant C_1.

(b) *The case $M_{11} = 1$ and $0 \leqslant M_{22} < 1$.* This is again the simple case of a free LW with exponential waiting time PDF, so that the MSD asymptotically scales linearly in time,

$$\langle x^2(t) \rangle \sim \frac{2v_0^2}{\lambda_1} t. \tag{55}$$

(c) *The case $0 \leqslant M_{11} < 1$ and $M_{22} = 1$.* Localisation is also obtained in this case, where the MSD is dominated by the trapping potential,

$$\langle x^2(t) \rangle \sim \frac{v_0^2}{\omega^2}. \tag{56}$$

Figure 7. MSD versus time t on log–log scale from stochastic simulations when both PDFs $\phi^{(2)}(\tau)$ and $\phi^{(1)}(\tau)$ have asymptotic power-law forms with $\alpha_1, \alpha_2 \in (0, 1)$. The numerical results are obtained from averaging over 2×10^4 realisations. The parameters are $\boldsymbol{\xi} = (0.5, 0.5)^{\mathrm{T}}$, $v_0 = 1$, $\omega = 1$. The stars represent the combination $\alpha_1 = 0.3$, $\alpha_2 = 0.7$, and $M_{11} = M_{22} = 0.5$ of the parameters. The full purple line corresponds to the theoretical result (59). The squares represent simulations with $\alpha_1 = 0.7$, $\alpha_2 = 0.3$, and the same choice of M_{11}, M_{22}, the corresponding theoretical result is (58). The circles correspond to simulations with $\alpha_1 = 0.7$, $\alpha_2 = 0.3$, and $M_{11} = 0.5$, $M_{22} = 1$, the associated theoretical result is equation (60) shown as full black line.

(d) *The case $M_{11} = M_{22} = 1$.* For the independent motion case we again find normal diffusion,

$$\langle x^2(t) \rangle \sim \frac{2v_0^2 \xi^{(1)}}{\lambda_1} t, \tag{57}$$

with the coefficient $\xi^{(1)}$.

3.2.2. The PDF $\phi^{(1)}(\tau)$ is an asymptotic power-law with divergent mean
When the waiting time PDF $\phi^{(1)}(\tau)$ has the asymptotic power-law shape (40) with $0 < \alpha_1 < 1$, the characteristic waiting time diverges. The asymptotic behaviours of the Laplace transforms $\mathscr{L}_\tau \left\{ \cos^2(\omega\tau)\phi^{(2)}(\tau) \right\}(s)$, $\mathscr{L}_\tau \left\{ \sin^2(\omega\tau)\phi^{(2)}(\tau) \right\}(s)$, and $\mathscr{L}_\tau \left\{ \sin^2(\omega\tau)\Psi^{(2)}(\tau) \right\}(s)$ are obtained in equations (D6), (D7), and (D9), respectively. We can then distinguish our four cases:

(a) *The case $0 \leqslant M_{11}, M_{22} < 1$.* Following the calculations in appendix D, we find superdiffusion for the case $0 \leqslant M_{11}, M_{22} < 1$ when both PDFs $\phi^{(1)}(\tau)$ and $\phi^{(2)}(\tau)$ have diverging mean but the tail of the soft-reset period is longer, i.e. $0 < \alpha_2 < \alpha_1 < 1$,

$$\langle x^2(t) \rangle \sim \frac{(1 - M_{22})\Gamma(3 - \alpha_1)v_0^2}{(1 - M_{11})\Gamma(1 - \alpha_2)\Gamma(3 - \alpha_1 + \alpha_2)} t^{2 - \alpha_1 + \alpha_2}. \tag{58}$$

The resulting exponent $2 - \alpha_1 + \alpha_2$ underlines the competition between the soft-reset trapping duration and the LW waiting times. Conversely, when $0 < \alpha_1 < \alpha_2 < 1$ or $1 < \alpha_2 < 2$, the LW motion dominates the spreading dynamics and we obtain ballistic motion weighted by the respective scaling exponents,
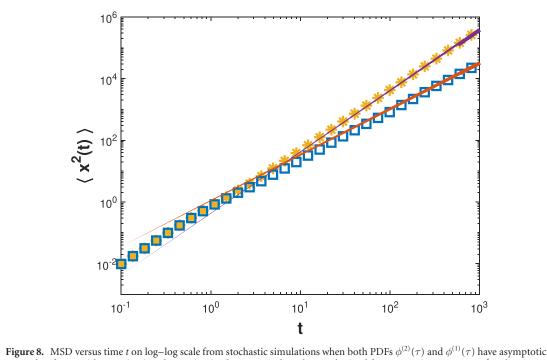
$$\langle x^2(t) \rangle \sim \frac{1}{2}(1 - \alpha_1)(2 - \alpha_1)v_0^2 t^2. \tag{59}$$

Both results are verified in figures 7 and 8 from stochastic simulations.
(b) *The case $M_{11} = 1$ and $0 \leqslant M_{22} < 1$.* For the free LW case the asymptotic behaviour of the MSD is the same as equation (43) for $\alpha_2 \in (0, 1)$.
(c) *The case $0 \leqslant M_{11} < 1$ and $M_{22} = 1$.* When $\alpha_2 \in (0, 1)$ and $\alpha_2 \in (1, 2)$, for the case $0 \leqslant M_{11} < 1$ and $M_{22} = 1$ we obtain superdiffusion of the form

$$\langle x^2(t) \rangle \sim \frac{2M_{11} v_0^2 \xi^{(1)}}{1 - M_{11}} t^{2 - \alpha_1}, \tag{60}$$

Figure 8. MSD versus time t on log–log scale from stochastic simulations when both PDFs $\phi^{(2)}(\tau)$ and $\phi^{(1)}(\tau)$ have asymptotic power-law forms with $\alpha_1 \in (0,1)$ and $\alpha_2 \in (1,2)$. The numerical results are obtained from averaging over 2×10^4 realisations. The parameters are $\alpha_1 = 0.5$, $\alpha_2 = 1.5$, $\boldsymbol{\xi} = (0.5, 0.5)^{\mathrm{T}}$, $v_0 = 1$, and $\omega = 1$. The stars represent the parameters $M_{11} = M_{22} = 0.5$, the full purple line represents the theoretical result (59). The squares correspond to $M_{11} = 0.5$ and $M_{22} = 1$, the theoretical result is given by equation (60) shown as the full red line.

whose scaling exponent solely depends on the waiting time exponent α_1. This result is confirmed from stochastic simulations in figures 7 and 8.

(d) *The case $M_{11} = M_{22} = 1$.* Finally, the independent case follows the asymptotic behaviour (46) for both $\alpha_2 \in (0,1)$ and $\alpha_2 \in (1,2)$.

3.2.3. The PDF $\phi^{(1)}(\tau)$ has asymptotic power-law form with finite mean but diverging second moment
We complete our analysis of the soft-reset LW process for the case when $\phi^{(1)}(\tau)$ has an asymptotic power-law form with scaling exponent $1 < \alpha_1 < 2$.

(a) *The case $0 \leqslant M_{11}, M_{22} < 1$.* In this case the long time dependence of the MSD is superdiffusive,

$$\langle x^2(t) \rangle \sim Ct^{3-\alpha_1} \tag{61}$$

when both $\alpha_2 \in (0,1)$ and $\alpha_2 \in (1,2)$.

For this case we also consider the asymptotic behaviour of the PDF $p(x,t)$. According to the stochastic simulations figure 9(a) we conclude that for $\alpha_2 \in (0,1)$ the asymptotic behaviour follows the power-law

$$p(x,t) \sim \frac{1}{|x|^{\alpha_1 + 0.4}}, \tag{62}$$

at both intermediate and large values of $|x|$. Due to the absence of a crossover the PDF for this case is therefore different from result (49) above, whereas when $\alpha_2 \in (1,2)$ according to the numerical simulation shown in figure 9(b) we find different asymptotic behaviours for different regions of x, specifically

$$p(x,t) \sim \begin{cases} \dfrac{1}{|x|^{\alpha_1 + (\alpha_2 - 1)/2}} & \text{for intermediate values of } |x|, \\[2mm] \dfrac{1}{|x|^{\alpha_1 - (\alpha_2 - 1)/2}} & \text{for large values of } |x|. \end{cases} \tag{63}$$
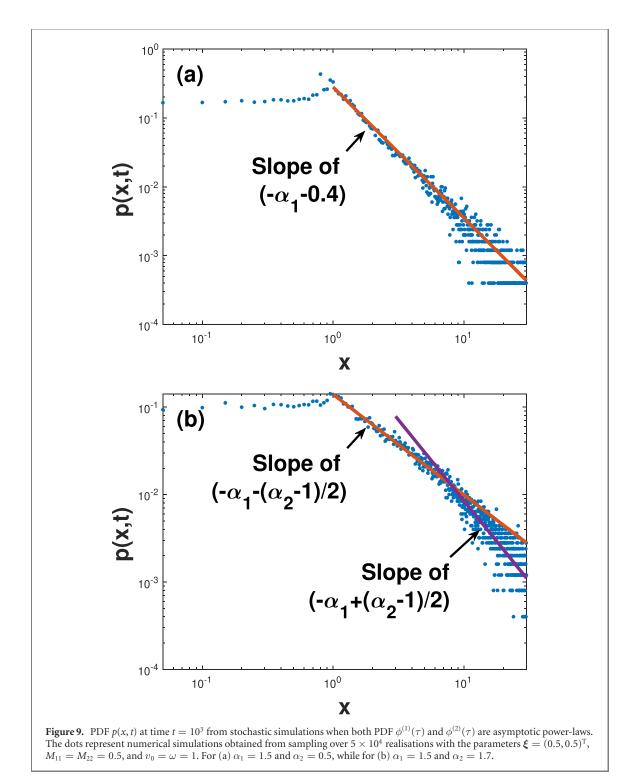
According to this conjecture the combined slope of both power-laws is $2\alpha_1$.

(b) *The case $M_{11} = 1$, $0 \leqslant M_{22} < 1$.* For pure LWs, as expected, the result for the MSD is given by the previous equation (50).

(c) *The case $0 \leqslant M_{11} < 1$ and $M_{22} = 1$.* Localisation is obtained in the case $0 \leqslant M_{11} < 1$ and $M_{22} = 1$, when $\phi^{(1)}(\tau)$ has a finite mean waiting time,

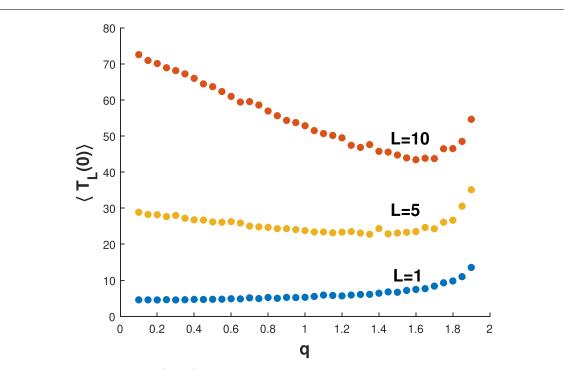$$\langle x^2(t) \rangle \sim C \tag{64}$$

for both $\alpha_2 \in (0,1)$ and $\alpha_2 \in (1,2)$.

Figure 9. PDF $p(x,t)$ at time $t = 10^3$ from stochastic simulations when both PDF $\phi^{(1)}(\tau)$ and $\phi^{(2)}(\tau)$ are asymptotic power-laws. The dots represent numerical simulations obtained from sampling over 5×10^4 realisations with the parameters $\boldsymbol{\xi} = (0.5, 0.5)^{\mathrm{T}}$, $M_{11} = M_{22} = 0.5$, and $v_0 = \omega = 1$. For (a) $\alpha_1 = 1.5$ and $\alpha_2 = 0.5$, while for (b) $\alpha_1 = 1.5$ and $\alpha_2 = 1.7$.
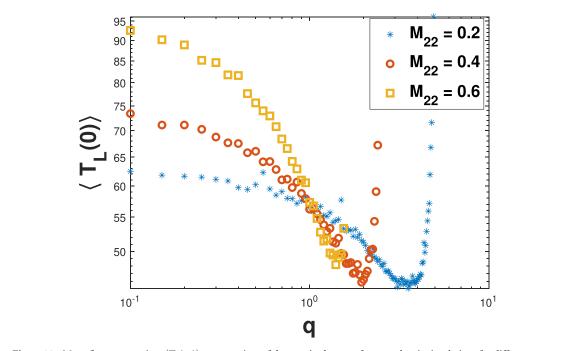
(d) *The case $M_{11} = M_{22} = 1$.* For independent processes the MSD follows equation (52). We summarise our results for the MSD when $\phi^{(2)}(\tau)$ has an asymptotic power-law from in table 2.

4. First-passage time dynamics

The first-passage time is one of the central statistic of stochastic processes [63, 64]. It quantifies when a stochastic variable first reaches a given value, relevant for, inter alia, molecular chemical reactions, financial transactions, or successful search processes. For LFs first-passage statistics and leapovers across the target were obtain in [56, 65, 66]. Results for asymmetric LFs were reported in [67, 68], while combined dynamics of LFs and Brownian motion, multiple targets, and LFs in external fields were analysed in [12, 69, 70]. LW first-passage were studied in [56, 71].
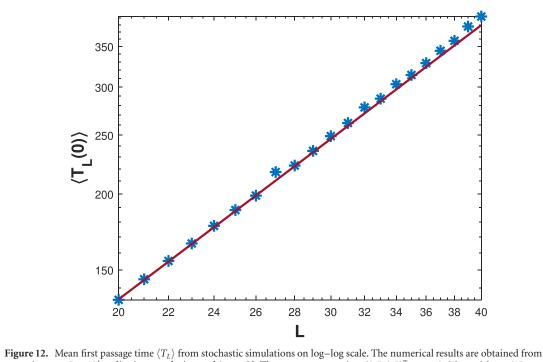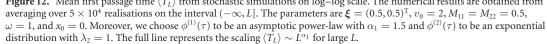
Figure 10. Mean first passage time $\langle T_L(x_0)\rangle$ versus ratio q of the matrix elements from stochastic simulations for different choices of L. The numerical results are obtained from averaging over 5×10^4 realisations on the interval $(-\infty, L]$. The parameters are $\boldsymbol{\xi} = (0.5, 0.5)^{\mathrm{T}}$, $v_0 = 2$, $\omega = 1$, $x_0 = 0$, and $M_{22} = 0.5$. Moreover we choose the PDF $\phi^{(1)}(\tau)$ to be of asymptotic power-law form with $\alpha_1 = 1.5$, and the PDF $\phi^{(2)}$ is an exponential distribution with $\lambda_2 = 1$.

Figure 11. Mean first passage time $\langle T_L(x_0)\rangle$ versus ratio q of the matrix elements from stochastic simulations for different choices of M_{22}. The numerical results are obtained from averaging over 5×10^4 realisations on the interval $(-\infty, L]$ with $L = 10$. The parameters are $\boldsymbol{\xi} = (0.5, 0.5)^{\mathrm{T}}$, $v_0 = 2$, $\omega = 1$, and $x_0 = 0$. Moreover we choose the PDFs $\phi^{(1)}(\tau)$ and $\phi^{(2)}(\tau)$ to be of asymptotic power-law forms with $\alpha_1 = 1.5$ and $\alpha_2 = 1.8$, respectively.

We here investigate the first-passage behaviour for soft-reset LWs. We denote by $T_L(x_0)$ the first time when the stochastic process starting at point x_0 first reaches a boundary at $L > 0$. The first-passage time for the traditional LW on a finite domain is discussed in [56]. Here we will utilise numerical simulations to calculate the mean first passage time $\langle T_L(x_0)\rangle$ with $x_0 = 0$, and the corresponding PDF $\varphi(T) = \langle \delta_{\mathrm{D}}(T_L(0) - T)\rangle$. In the associated one-dimensional domain $(-\infty, L]$, it will take a long time for an

Figure 12. Mean first passage time $\langle T_L \rangle$ from stochastic simulations on log–log scale. The numerical results are obtained from averaging over 5×10^4 realisations on the interval $(-\infty, L]$. The parameters are $\boldsymbol{\xi} = (0.5, 0.5)^{\mathrm{T}}$, $v_0 = 2$, $M_{11} = M_{22} = 0.5$, $\omega = 1$, and $x_0 = 0$. Moreover, we choose $\phi^{(1)}(\tau)$ to be an asymptotic power-law with $\alpha_1 = 1.5$ and $\phi^{(2)}(\tau)$ to be an exponential distribution with $\lambda_2 = 1$. The full line represents the scaling $\langle T_L \rangle \sim L^{\alpha_1}$ for large L.

ordinary LW particle to reach the boundary L. In order to improve the search efficiency and reduce the first passage time, the concept of 'resetting' is often invoked, which means to return the particle to some point after a given search time [35, 58, 72]. It can be found that the random harmonic potential in our soft-resetting scenario has a similar beneficial effect on the LW search.

First we discuss the effect of the entries of the transition matrix on the mean first passage time $\langle T_L(0) \rangle$, for which we define the ratio $q = M_{11}/M_{22}$ with $0 < M_{11}, M_{22} < 1$. Thus q is less than $\frac{1}{M_{22}}$. We here only consider the cases when the waiting time PDF $\phi^{(1)}(\tau)$ is an asymptotic power-law with $1 < \alpha_1 < 2$, the most standard LW scenario, together with the soft-reset period PDF $\phi^{(2)}(\tau)$ of either exponential or asymptotic power-law shape with $1 < \alpha_2 < 2$. A more extensive study of the first-passage dynamics of soft-reset LWs for the entire parameters space will be the focus of another report.

From the stochastic simulations shown in figure 10 we find that there exists some optimal ratio q^* that minimises the mean first passage time $\langle T_L(x_0) \rangle$ as long as the boundary is a sufficient distance L away. In this case, for $q < q^*$ the mean first passage time decreases approximately linearly with increasing q, while $\langle T_L(x_0) \rangle$ increases more quickly when $q > q^*$. Moreover we see from figure 11 that the optimal value of q, q^*, depends on the value of M_{22}: when M_{22} is smaller, q^* is reduced.

These results indicate that for the domain $(-\infty, L]$ the most efficient search strategy for an LW process is given in the presence of stochastic soft-reset events. For large L, from the simulations in figure 12 we find that $\langle T_L(0) \rangle \sim L^{\alpha_1}$.
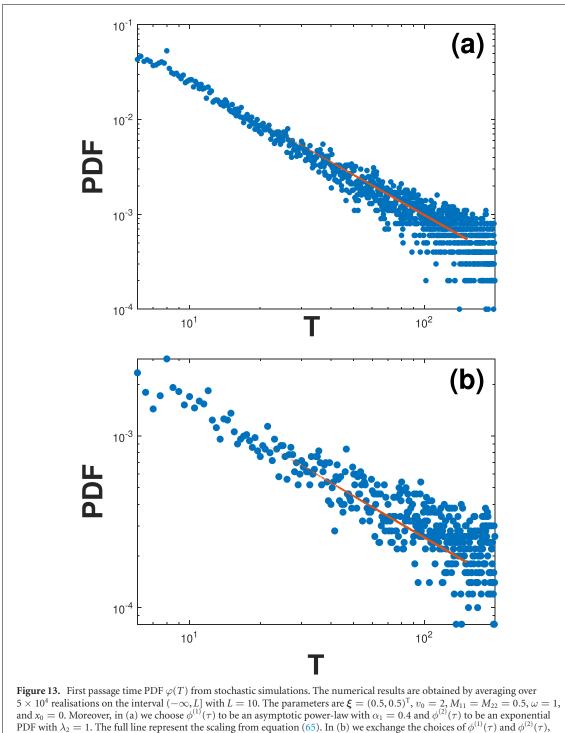
Next, we consider the PDF $\phi(T)$ of first passage times. From stochastic simulations we obtain the asymptotic behaviours for different cases. First when $\phi^{(1)}(\tau)$ is an asymptotic power-law with $0 < \alpha_1 < 1$, and $\phi^{(2)}(\tau)$ has a finite average, when $0 < M_{11}, M_{22} < 1$ we find that

$$\varphi(T) \simeq T^{-1-\alpha_1}, \tag{65}$$

for sufficiently large L and T. Additionally, when the mean of the density $\phi^{(1)}(\tau)$ is finite and $\phi^{(2)}(\tau)$ is an asymptotic power-law with $0 < \alpha_2 < 1$, under the same conditions $0 < M_{11}, M_{22} < 1$ the first-passage PDF asymptotically scales like

$$\varphi(T) \simeq T^{-1+\alpha_2/2}. \tag{66}$$

The results of equations (65) and (66) are in line with the stochastic simulations in figure 13.

Figure 13. First passage time PDF $\varphi(T)$ from stochastic simulations. The numerical results are obtained by averaging over 5×10^4 realisations on the interval $(-\infty, L]$ with $L = 10$. The parameters are $\boldsymbol{\xi} = (0.5, 0.5)^{\mathrm{T}}$, $v_0 = 2$, $M_{11} = M_{22} = 0.5$, $\omega = 1$, and $x_0 = 0$. Moreover, in (a) we choose $\phi^{(1)}(\tau)$ to be an asymptotic power-law with $\alpha_1 = 0.4$ and $\phi^{(2)}(\tau)$ to be an exponential PDF with $\lambda_2 = 1$. The full line represent the scaling from equation (65). In (b) we exchange the choic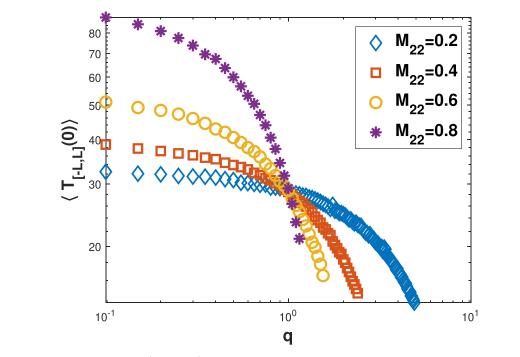es of $\phi^{(1)}(\tau)$ and $\phi^{(2)}(\tau)$, and the corresponding asymptotic scaling of $\varphi(T)$ is given by equation (66).

Finally, we determine the mean first-passage time on the finite domain $[-L, L]$, denoted as $\langle T_{[-L,L]}(x_0) \rangle$ with start position $x_0 = 0$. With the same definition of the ratio q, we simulate $\langle T_{[-L,L]}(x_0) \rangle$ versus q. From the simulations results in figure 14 we find a totally different behaviour in which $\langle T_{[-L,L]}(x_0) \rangle$ is simply a decreasing function of q. Not unexpectedly, in the finite-domain scenario resets do not effect an optimal behaviour. In fact, when the domain is finite, the best effect is when the random harmonic potential is weak or absent.

5. Conclusion

We here developed and analysed an LW model in the presence of stochastic soft-resetting events by an harmonic potential, formulated in terms of multiple internal states. The switching between free LW motion and soft-reset events is described in terms of the transition matrix M while the durations of either phase are

Figure 14. Mean first passage time $\langle T_{[-L,L]]}(x_0) \rangle$ versus the ratio q. The numerical results are obtained from averaging over 5×10^4 realisations on the interval $[-L, L]$ with $L = 10$. The parameters are $\boldsymbol{\xi} = (0.5, 0.5)^{\mathrm{T}}$, $v_0 = 2$, $\omega = 1$, and $x_0 = 0$. Moreover we choose $\phi^{(1)}(\tau)$ and $\phi^{(1)}(\tau)$ to be power-law PDFs with scaling exponents $\alpha_1 = 1.5$ and $\alpha_2 = 1.8$, respectively.

defined by the respective PDFs $\phi^{(1)}(\tau)$ and $\phi^{(2)}(\tau)$. The solution was obtained from expansion in Hermite orthogonal polynomials, an effective method to deal with some problems in LW theory that cannot be solved by ordinary Fourier–Laplace transform. The waiting time PDF $\phi^{(1)}(\tau)$ here quantifies the duration of LW motion events while the PDF $\phi^{(2)}(\tau)$ reflects the length of the periods, during which the confining harmonic potential is switched on. The two effects of free motion and confinement compete against each other, and we unveiled a very rich behaviour of the particle spreading dynamics for specific choices of the PDFs $\phi^{(1)}(\tau)$ and $\phi^{(2)}(\tau)$.

Specifically, when $\phi^{(2)}(\tau)$ is an exponential PDF, the process is localised if $\phi^{(1)}(\tau)$ is also an exponential PDF with $M_{11}, M_{22} \in [0, 1)$. When $\phi^{(1)}(\tau)$ is an asymptotic power-law PDF with divergent second moment, the asymptotic behaviours of the MSDs witness that the stochastic harmonic potential has only a minor influence on the diffusion, by changing the prefactor of the MSD. Moreover, when $0 \leqslant M_{11} < 1$ and $M_{22} = 1$, it will be expected to observe particle localisation since this choice of M_{11} and M_{22} ends up with the result that all of particles stay in the confined state. However, when the average of $\phi^{(1)}(\tau)$ is divergent, we still obtain superdiffusion, a somewhat counter-intuitive result. The effect of the competition between free motion and the stochastic harmonic potential can be observed most directly when both $\phi^{(1)}(\tau)$ and $\phi^{(2)}(\tau)$ are asymptotic power-law distributions with $0 < \alpha_1, \alpha_2 < 1$. In this case, we find that when $\alpha_2 < \alpha_1$ and $0 \leqslant M_{11}, M_{22} < 0$, the MSD $\langle x^2(t) \rangle \sim t^{2-\alpha_1+\alpha_2}$ is superdiffusive, whereas ballistic motion is obtained when $\alpha_2 > \alpha_1$—in that case the free LW motion dominates.

For the soft-rest LW scenario we find that the stationary PDF in the NESS may acquire mono-modal or bimodal shapes depending on the specific choices of the parameters λ_1, v_0, and ω. Multimodal states have previously been observed for both LFs and LWs in external potentials [49, 53–55, 73]. However, multimodal states may also be observed in persistent long-ranged correlated processes such as superdiffusive fractional Brownian motion [74] and are an interesting phenomenon of their own right, deserving additional future attention.

Moreover, from the analysis of the kurtosis K, we discover that for $0 \leqslant M_{11}, M_{22} < 1$ the PDF can be leptokurtic or platykurtic, determined by the value of the inverse waiting time scale λ_1 for small inverse time scale λ_2 of the soft-reset periods. This phenomenon is completely different from LWs in a permanently acting harmonic potential case. Moreover, from the analysis of the asymptotic behaviours of the tails of PDFs, we also observe marked differences from the case of a constant harmonic confinement.

In the last part of this paper, we discuss the first passage time in terms of numerical simulations. First we define the ratio q as M_{11} over M_{22}, from the simulations we find that when we choose domain as $(-\infty, L]$ then the mean first passage time for large L can achieve a minimum for some q^*. However, when the domain is finite, $[-L, L]$, soft-resets do not effect optimal search dynamics.

We expect that the rich phase space of soft-reset LWs makes them an ideal candidate to quantify random search processes in the presence of soft resetting events.

Acknowledgments

Data availability statement

No new data were created or analysed in this study.

Appendix A. A brief introduction of Hermite orthogonal polynomials

Hermite polynomials $\{H_n(x)\}$ are orthogonal over $(-\infty, \infty)$ with respect to the weight function $w(x) = e^{-x^2}$ [75, 76],

$$\int_{-\infty}^{\infty} H_m(x)H_n(x)w(x)\mathrm{d}x = \sqrt{\pi}2^n n!\delta_{n,m}, \tag{A1}$$

where $\delta_{n,m}$ is the Kronecker δ symbol defined as

$$\delta_{n,m} = \begin{cases} 1 & \text{for } m = n \\ 0 & \text{for } m \neq n. \end{cases}$$

The Hermite polynomials are given by

$$H_n(x) = \begin{cases} n!\sum_{i=0}^{n/2} \dfrac{(-1)^{\frac{n}{2}-i}}{(2i)!\left(\frac{n}{2}-i\right)!}(2x)^{2i} & \text{for even } n; \\ n!\sum_{i=0}^{\frac{n-1}{2}} \dfrac{(-1)^{\frac{n-1}{2}-i}}{(2i+1)!\left(\frac{n-1}{2}-i\right)!}(2x)^{2i+1} & \text{for odd } n. \end{cases} \tag{A2}$$

The values of the Hermite polynomials at $x = 0$ are

$$H_n(0) = \begin{cases} \dfrac{(-1)^{n/2}n!}{(n/2)!} & \text{for even } n; \\ 0 & \text{for odd } n. \end{cases} \tag{A3}$$

Another two important properties for Hermite polynomials are

$$H_n(x + y) = \sum_{l=0}^{n} \binom{n}{l} H_l(x)(2y)^{n-l}, \tag{A4}$$

and

$$H_n(cx) = \sum_{k=0}^{\lfloor\frac{n}{2}\rfloor} c^{n-2k}(c^2 - 1)^k \binom{n}{2k} \frac{(2k)!}{k!}H_{n-2k}(x), \tag{A5}$$

where $\binom{n}{l} = \frac{n!}{l!(n-l)!}$ and $\lfloor\frac{n}{2}\rfloor$ is the floor function representing the biggest integer less than $n/2$. Further there exists the following Fourier transform [75]

$$\mathscr{F}_x\left\{H_n(x)e^{-x^2}\right\}(k) = \sqrt{\pi}(-\mathrm{i}k)^n \exp\left(-\frac{k^2}{4}\right). \tag{A6}$$

Appendix B. Derivations of equations (13) and (14)

In this part, we derive the recursion relations of $T_n^{(1,2)}(t)$. First we substitute the presumed form (12) into (10), then there exists

$$\sum_{n=0}^{\infty} H_n(x)e^{-x^2}T_n^{(1)}(t) = \frac{M_{11}}{2}\int_0^t\sum_{n=0}^{\infty}\left[H_n(x+v_0\tau)e^{-(x+v_0\tau)^2}\right.$$

$$\left. + H_n(x-v_0\tau)e^{-(x-v_0\tau)^2}\right]T_n^{(1)}(t-\tau)\phi^{(1)}(\tau)d\tau$$

$$+ \frac{M_{21}}{2}\int_0^t\sum_{n=0}^{\infty}\left[H_n(x+v_0\tau)e^{-(x+v_0\tau)^2} + H_n(x-v_0\tau)e^{-(x-v_0\tau)^2}\right]$$

$$\times T_n^{(2)}(t-\tau)\phi^{(1)}(\tau)d\tau + \xi^{(1)}\delta_D(x-x_0)\delta_D(t). \tag{B1}$$

Then the main procedure to deal with equation (B1) is to multiply with $H_m(x)$ and integrate with respect to x over $(-\infty, \infty)$ on both sides of (B1). Then the left-hand side of equation (B1) becomes

$$\sum_{n=0}^{\infty}\int_{-\infty}^{\infty}H_m(x)H_n(x)e^{-x^2}T_n^{(1)}(t)dx = \sqrt{\pi}2^m m!T_m^{(1)}(t), \tag{B2}$$

where the orthogonal property (A1) is used. For the right-hand side of equation (B1) the key issue to perform these procedures will be

$$\sum_{n=0}^{\infty}\int_{-\infty}^{\infty}H_n(x\pm v_0\tau)e^{-(x\pm v_0\tau)^2}H_m(x)dx = \sum_{n=0}^{\infty}\int_{-\infty}^{\infty}H_n(y)e^{-y^2}H_m(y\mp v_0\tau)dy$$

$$= \sum_{n=0}^{\infty}\sum_{k=0}^{m}\frac{m!(\mp2v_0\tau)^{m-k}}{k!(m-k)!}\int_{-\infty}^{\infty}H_n(y)H_k(y)e^{-y^2}\,dy$$

$$= \sum_{k=0}^{m}\frac{\sqrt{\pi}2^k m!(\mp2v_0\tau)^{m-k}}{(m-k)!},$$

where we utilise the properties (A4) and (A1) of the Hermite polynomials. Then the result of equation (13) can be easily obtained.

Equation (11) is more tricky to deal with. Building on the approach developed in [49] we have

$$\sum_{n=0}^{\infty}H_n(x)e^{-x^2}T_n^{(2)}(t) - \xi_2\delta_D(x-x_0)\delta_D(t) = \frac{M_{12}}{2}\int_0^t\sum_{n=0}^{\infty}\left[H_n(x_+)e^{-x_+^2} + H_n(x_-)e^{-x_-^2}\right]$$

$$\times T_n^{(1)}(t-\tau)\frac{\phi^{(2)}(\tau)}{|\cos(\omega\tau)|}\,d\tau$$

$$+ \frac{M_{22}}{2}\int_0^t\sum_{n=0}^{\infty}\left[H_n(x_+)e^{-x_+^2} + H_n(x_-)e^{-x_-^2}\right]$$

$$\times T_n^{(2)}(t-\tau)\frac{\phi^{(2)}(\tau)}{|\cos(\omega\tau)|}\,d\tau. \tag{B3}$$

Then we deal with equation (B3) with the same procedure performed on (B1), and the left-hand side is the same as (B2) expect for changing the first state to the second one. As for the right-hand side, the key issue is to calculate the following integral

$$\int_{-\infty}^{\infty}q^{(i)}(x_\pm, t-\tau)H_m(x)dx = \sum_{n=0}^{\infty}\frac{1}{|\cos(\omega\tau)|}\int_{-\infty}^{\infty}H_n(x_\pm)e^{-x_\pm^2}T_n^{(i)}(t-\tau)H_m(x)dx$$

$$= \sum_{n=0}^{\infty}\int_{-\infty}^{\infty}H_n(y)e^{-y^2}H_m\left(\cos(\omega\tau)y\mp\frac{v_0}{\omega}\sin(\omega\tau)\right)dy$$

$$\times T_n^{(i)}(t-\tau), \tag{B4}$$

where we change the variable in the second equation. Then from (A4) and (A5), we have

$$H_m\left(\cos(\omega\tau)y \mp \frac{v_0}{\omega}\sin(\omega\tau)\right) = \sum_{l=0}^{m}\frac{m!}{l!(m-l)!}H_l\left(\cos(\omega\tau)y\right)\left(\mp\frac{2v_0}{\omega}\sin(\omega\tau)\right)^{m-l}$$

$$= \sum_{l=0}^{m}\frac{m!}{l!(m-l)!}\sum_{k=0}^{\lfloor\frac{l}{2}\rfloor}\cos^{l-2k}(\omega\tau)(\cos^2(\omega\tau)-1)^k \qquad (B5)$$

$$\times \frac{l!}{k!(l-2k)!}H_{l-2k}(y)\left(\mp\frac{2v_0}{\omega}\sin(\omega\tau)\right)^{m-l}.$$

Substituting (B5) into (B4) and with the help of (A1) we have

$$\int_{-\infty}^{\infty}q^{(i)}(x_\pm, t-\tau)H_m(x)dx = \sum_{l=0}^{m}\sum_{k=0}^{\lfloor\frac{l}{2}\rfloor}\frac{\sqrt{\pi}2^{l-2k}\,m!}{k!(m-l)!}\cos^{l-2k}(\omega\tau)\left(\cos^2(\omega\tau)-1\right)^k$$

$$\times\left(\mp\frac{2v_0}{\omega}\sin(\omega\tau)\right)^{m-l}T_{l-2k}^{(i)}(t-\tau). \qquad (B6)$$

Therefore, after multiplying with $H_m(x)$ and integrating with respect to x over the whole space on both sides of (11), and further from (B6) we have the recursion relation (14).

Appendix C. Expression for the kurtosis

The exact expression for the kurtosis reads

$$K \sim \Big[3\lambda_1^4(-1+M_{11})^2(\lambda_1(-1+M_{11})+\lambda_2(-1+m_22))^2\omega^4\Big(1+\Big(2\left(\lambda_1^3(-1+M_{11})^2(2v_0^2-\omega^2)\right.$$
$$+\lambda_1^2\lambda_2(-1+M_{11})(-1+M_{22})(2v_0^2-\omega^2)+2\lambda_1(-1+M_{11})(-1+M_{22})v_0^2(\lambda_2^2+2\omega^2)$$
$$+\,2\lambda_2(-1+M_{22})v_0^2(\lambda_2^2(-1+M_{22})+2(-2+M_{22})\omega^2))\Big)\Big/\left(\lambda_1^2(-1+M_{11})\left(\lambda_1(-1+M_{11})\right.\right.$$
$$+\,\lambda_2(-1+M_{22}))\,\omega^2\right)+\left(\lambda_1(-1+M_{11})\left(4\lambda_1^2(-1+M_{11})(-1+M_{22})v_0^2(2v_0^2-\omega^2)\right.\right.$$
$$\times(\lambda_2^4+12\lambda_2^2\omega^2+20\omega^4)+4(-1+M_{22})v_0^4(\lambda_2^2(-1+M_{22})+2(-2+M_{22})\omega^2)$$
$$\times\,(\lambda_2^4+16\lambda_2^2\omega^2+24\omega^4)+\lambda_1^4(-1+M_{11})^2(24v_0^4\omega^2-40v_0^2\omega^4+10\omega^6+\lambda_2^2(-2v_0^2+\omega^2)^2))$$
$$+\lambda_2(-1+M_{22})\left(4\lambda_1^2(-1+M_{11})v_0^2(2v_0^2-\omega^2)(\lambda_2^2+10\omega^2)(\lambda_2^2(-1+M_{22})+2(-2+M_{22})\omega^2)\right.$$
$$+4v_0^4\left(\lambda_2^6(-1+M_{22})^2+6\lambda_2^4(4-7M_{22}+3M_{22}^2)\omega^2+8\lambda_2^2(18-24M_{22}+7M_{22}^2)\omega^4\right.$$
$$+\,16(16-14M_{22}+3M_{22}^2)\omega^6)+\lambda_1^4(-1+M_{11})^2\left(24v_0^4\omega^2-40v_0^2\omega^4+10\omega^6\right.$$
$$+\,\lambda_2^2(-2v_0^2+\omega^2)^2)))\Big/(\lambda_1^4(-1+M_{11})^2(\lambda_1(-1+M_{11})+\lambda_2(-1+M_{22}))\omega^4(\lambda_2^2+10\omega^2)))\Big]$$
$$\Big/\Big[4v_0^4\left(\lambda_1^3(-1+M_{11})^2+\lambda_1^2\lambda_2(-1+M_{11})(-1+M_{22})+\lambda_1(-1+M_{11})(-1+M_{22})(\lambda_2^2+2\omega^2)\right.$$
$$+\,\lambda_2(-1+M_{22})(\lambda_2^2(-1+M_{22})+2(-2+M_{22})\omega^2))^2\Big].$$

Appendix D. Derivations of equations (58) and (59)

In order to calculate the MSD when both $\phi^{(1)}(\tau)$ and $\phi^{(2)}(\tau)$ are asymptotic power-law PDFs, i.e. of the form $\phi^{(i)}(\tau) = \alpha_i(1+\tau)^{-1-\alpha_i}$, some Laplace transforms are useful when we consider equation (26). The first Laplace transform required is

$$\mathscr{L}_\tau\left\{\cos^2(\omega\tau)\phi^{(2)}(\tau)\right\}(s) = \frac{\alpha_2}{2}e^s E_{1+\alpha_2}(s) + \frac{\alpha_2}{4}e^{s-2i\omega}E_{1+\alpha_2}(s-2i\omega) + \frac{\alpha_2}{4}e^{s+2i\omega}E_{1+\alpha_2}(s+2i\omega), \qquad (D1)$$

where $E_\beta(x) = \int_1^\infty\frac{e^{-xt}}{t^\beta}dt$ is the exponential integral. Next take a Taylor expansion on the right-hand side of (D1) and ignore the higher order terms. Then the first term reads

$$\frac{\alpha_2}{2}e^s E_{1+\alpha_2}(s) \sim \frac{1}{2} + \frac{s}{2(1-\alpha_2)} + \frac{\alpha_2}{2}\Gamma(-\alpha_2)s^{\alpha_2}. \qquad (D2)$$

Further, the following relation is needed to calculate the Taylor expansion of next two terms of (D1),

$$
\begin{aligned}
e^{-2i\omega}E_{1+\alpha_2}(-2i\omega) + e^{2i\omega}E_{1+\alpha_2}(2i\omega) &= \int_1^\infty \frac{e^{-2i\omega(t+1)}}{t^{1+\alpha_2}}\,dt + \int_1^\infty \frac{e^{2i\omega(t+1)}}{t^{1+\alpha_2}}\,dt \\
&= 2\int_1^\infty \frac{\cos(2\omega(t+1))}{t^{1+\alpha_2}}\,dt \\
&= 2\mathcal{I}_{\alpha_2+1}(\omega),
\end{aligned}
\tag{D3}
$$

where

$$
\mathcal{I}_\beta(\omega) = \int_1^\infty \frac{\cos(2\omega(t+1))}{t^\beta}\,dt.
\tag{D4}
$$

Then

$$
\begin{aligned}
e^{s-2i\omega}E_{1+\alpha_2}(s-2i\omega) + e^{s+2i\omega}E_{1+\alpha_2}(s+2i\omega) &\sim \left(e^{-2i\omega}E_{1+\alpha_2}(-2i\omega) + e^{2i\omega}E_{1+\alpha_2}(2i\omega)\right) \\
&\quad + s\left(-e^{-2i\omega}E_{\alpha_2}(-2i\omega) + e^{-2i\omega}E_{1+\alpha_2}(-2i\omega)\right) \\
&\quad + s\left(-e^{2i\omega}E_{\alpha_2}(2i\omega) + e^{2i\omega}E_{1+\alpha_2}(2i\omega)\right) \\
&= 2\mathcal{I}_{\alpha_2+1}(\omega) + 2\left(\mathcal{I}_{\alpha_2}(\omega) + \mathcal{I}_{\alpha_2+1}(\omega)\right)s.
\end{aligned}
\tag{D5}
$$

Finally, from (D1) there exists

$$
\begin{aligned}
\mathscr{L}_\tau\left\{\cos^2(\omega\tau)\phi^{(2)}(\tau)\right\}(s) &\sim \frac{1}{2} + \frac{\alpha_2}{2}\mathcal{I}_{\alpha_2+1}(\omega) + \left(\frac{1}{2(1-\alpha_2)} - \frac{\alpha_2}{2}\mathcal{I}_{\alpha_2}(\omega) - \frac{\alpha_2}{2}\mathcal{I}_{\alpha_2+1}(\omega)\right)s \\
&\quad + \frac{\alpha_2}{2}\Gamma(-\alpha_2)s^{\alpha_2}
\end{aligned}
\tag{D6}
$$

Similarly, we have

$$
\begin{aligned}
\mathscr{L}_\tau\left\{\sin^2(\omega\tau)\phi^{(2)}(\tau)\right\}(s) &= \frac{\alpha_2}{2}e^s E_{1+\alpha_2}(s) - \frac{\alpha_2}{4}\left[e^{s-2i\omega}E_{1+\alpha_2}(s-2i\omega) + e^{s+2i\omega}E_{1+\alpha_2}(s+2i\omega)\right] \\
&\sim \frac{1}{2} - \frac{\alpha_2}{2}\mathcal{I}_{\alpha_2+1}(\omega) + \frac{\alpha_2}{2}\Gamma(-\alpha_2)s^{\alpha_2} \\
&\quad + \left(\frac{1}{2(1-\alpha_2)} - \frac{\alpha_2}{2}\mathcal{I}_{\alpha_2}(\omega) - \frac{\alpha_2}{2}\mathcal{I}_{\alpha_2+1}(\omega)\right)s.
\end{aligned}
\tag{D7}
$$

Additionally, the survival probability of $\phi^{(2)}(\tau)$ is

$$
\Psi^{(2)}(\tau) = \int_\tau^\infty \alpha_2(1+\tau')^{-1-\alpha_2}\,d\tau' = (1+\tau)^{-\alpha_2}.
\tag{D8}
$$

Then

$$
\begin{aligned}
\mathscr{L}_\tau\left\{\sin^2(\omega\tau)\Psi^{(2)}(\tau)\right\}(s) &= \frac{1}{2}e^s E_{\alpha_2}(s) + \frac{1}{4}\left[e^{s-2i\omega}E_{\alpha_2}(s-2i\omega) + e^{s+2i\omega}E_{\alpha_2}(s+2i\omega)\right] \\
&\sim \frac{1}{2(\alpha_2-1)} + \frac{1}{2}\mathcal{I}_{\alpha_2+1}(\omega) + \frac{1}{2}\Gamma(1-\alpha_2)s^{\alpha_2-1} \\
&\quad + \frac{1}{2}\left(\frac{1}{2-\alpha_2} - \frac{1}{\alpha_2-1} + \mathcal{I}_{\alpha_2}(\omega) - \mathcal{I}_{\alpha_2-1}(\omega)\right)s.
\end{aligned}
\tag{D9}
$$

Choosing $0 \leqslant M_{11}, M_{22} < 1$ and $0 < \alpha_2 < \alpha_1 < 1$, then from (15) we have

$$\widehat{T}_0^{(1)}(s) \sim \mathcal{O}(s^{-\alpha_2}), \tag{D10}$$

where we borrow the notation $\mathcal{O}(s^{-\alpha_2})$ to represent $Cs^{-\alpha_2}$ with the constant C. Moreover, from (16) we have

$$\widehat{T}_0^{(2)}(s) \sim \mathcal{O}(s^{-\alpha_2}). \tag{D11}$$

Although for $\widehat{T}_0^{(1)}(s)$ and $\widehat{T}_0^{(2)}(s)$ the order of s are the same, so that the symbols may seem the same, the constants are different. Again by solving (15) and (16) with $n = 2$, and utilising (D6), (D7) there exists

$$\widehat{T}_2^{(1)}(s) \sim \mathcal{O}(s^{-\alpha_2}),$$
$$\widehat{T}_2^{(2)}(s) \sim \mathcal{O}(s^{-2+\alpha_1-\alpha_2}). \tag{D12}$$

Then from (18) and (19), and (D9) we have

$$\widehat{R}_2^{(1)}(s) \sim \mathcal{O}(s^{-3+\alpha_1-\alpha_2}),$$
$$\widehat{R}_2^{(2)}(s) \sim \mathcal{O}(s^{-3+\alpha_1}). \tag{D13}$$

Finally from (26), we have

$$\langle x^2(s) \rangle \sim \mathcal{O}(s^{-3+\alpha_1-\alpha_2}), \tag{D14}$$

whose inverse Laplace transform is given by

$$\langle x^2(t) \rangle \sim t^{2-\alpha_1+\alpha_2}. \tag{D15}$$

In contrast, when we choose $0 < \alpha_1 < \alpha_2 < 1$, with similar calculations

$$\widehat{T}_0^{(1)}(s) \sim \mathcal{O}(s^{-\alpha_1}), \qquad \widehat{T}_0^{(2)}(s) \sim \mathcal{O}(s^{-\alpha_1})$$
$$\widehat{T}_2^{(1)}(s) \sim \mathcal{O}(s^{-2}), \qquad \widehat{T}_0^{(2)}(s) \sim \mathcal{O}(s^{-2}), \tag{D16}$$

further

$$\widehat{R}_2^{(1)}(s) \sim \mathcal{O}(s^{-3}), \qquad \widehat{R}_2^{(1)}(s) \sim \mathcal{O}(s^{-3+\alpha_2}). \tag{D17}$$

Thus we have $\langle x^2(t) \rangle \sim t^2$.

Finally when $1 < \alpha_1 < 2$, and $0 < \alpha_2 < 1$, with the same conditions on M_{11}, M_{22}, it can be obtained that $\langle x^2(t) \rangle \sim t^{3-\alpha_1}$.

ORCID iDs

Ralf Metzler ⬤ https://orcid.org/0000-0002-6013-7020
Weihua Deng ⬤ https://orcid.org/0000-0002-8573-012X

References

[1] Mandelbrot B B 1982 *The Fractal Geometry of Nature* (San Francisco, CA: Freeman)
[2] Mandelbrot B 1963 The variation of certain speculative prices *J. Bus.* **36** 394
[3] Sokolov I M, Mai J and Blumen A 1997 Paradoxal diffusion in chemical space for nearest-neighbor walks over polymer chains *Phys. Rev. Lett.* **79** 857
[4] Lomholt M A, Ambjörnsson T and Metzler R 2005 Optimal target search on a fast-folding polymer chain with volume exchange *Phys. Rev. Lett.* **95** 260603
[5] Shlesinger M F, Klafter J and Wong Y M 1982 Random walks with infinite spatial and temporal moments *J. Stat. Phys.* **27** 499
[6] Shlesinger M F and Klafter J 1986 *On Growth and Form* ed H E Stanley and N Ostrowsky (Dordrecht: Martinus Nijhoff)
[7] Viswanathan G M, Buldyrev S V, Havlin S, da Luz M G E, Raposo E P and Stanley H E 1999 Optimizing the success of random searches *Nature* **401** 911
[8] Bartumeus F, Catalan J, Fulco U L, Lyra M L and Viswanathan G M 2002 Optimizing the encounter rate in biological interactions: Lévy versus Brownian strategies *Phys. Rev. Lett.* **88** 097901
[9] Lomholt M A, Tal K, Metzler R and Joseph K 2008 Levy strategies in intermittent search processes are advantageous *Proc. Natl Acad. Sci.* **105** 11055
[10] Pavlyukevich I 2007 Lévy flights, non-local search and simulated annealing *J. Comput. Phys.* **226** 1830
[11] Viswanathan G M, da Luz M G E, Raposo E P and Stanley H E 2011 *The Physics of Foraging: An Introduction to Random Searches and Biological Encounters* (Cambridge: Cambridge University Press)
[12] Palyulin V V, Chechkin A V and Metzler R 2014 Levy flights do not always optimize random blind search for sparse targets *Proc. Natl Acad. Sci.* **111** 2931
[13] Levernier N, Textor J, Bénichou O and Voituriez R 2020 Inverse square Lévy walks are not optimal search strategies for $d \geqslant 2$ *Phys. Rev. Lett.* **124** 080601

[14] Reynolds A 2015 Liberating Lévy walk research from the shackles of optimal foraging *Phys. Life Rev.* **14** 59

[15] Humphries N E, Weimerskirch H, Queiroz N, Southall E J and Sims D W 2012 Foraging success of biological Levy flights recorded *in situ Proc. Natl Acad. Sci.* **109** 7169

[16] Sims D W *et al* 2008 Scaling laws of marine predator search behaviour *Nature* **451** 1098

[17] Raichlen D A, Wood B M, Gordon A D, Mabulla A Z P, Marlowe F W and Pontzer H 2014 Evidence of Levy walk foraging patterns in human hunter-gatherers *Proc. Natl Acad. Sci.* **111** 728

[18] Murakami H, Feliciani C and Nishinari K 2019 Lévy walk process in self-organization of pedestrian crowds *J. R. Soc. Interface.* **16** 20180939

[19] Brockmann D, Hufnagel L and Geisel T 2006 The scaling laws of human travel *Nature* **439** 462
Reynolds A, Ceccon E, Baldauf C, Karina Medeiros T and Miramontes O 2018 Lévy foraging patterns of rural humans *PLoS One* **13** e0199099

[20] Gross B, Zheng Z, Liu S, Chen X, Sela A, Li J, Li D and Havlin S 2020 Spatio-temporal propagation of COVID-19 pandemics *EPL* **131** 58003

[21] Fioriti V, Fratichini F, Chiesa S and Moriconi C 2015 Levy foraging in a dynamic environment—extending the Levy search *Int. J. Adv. Robot. Syst.* **12** 98
Katada Y, Nishiguchi A, Moriwaki K and Watakabe R 2016 Swarm robotic network using Lévy flight in target detection problem *Artif. Life Robot.* **21** 295

[22] Chen K, Wang B and Granick S 2015 Memoryless self-reinforcing directionality in endosomal active transport within living cells *Nat. Mater.* **14** 589

[23] Song M S, Moon H C, Jeon J-H and Park H Y 2018 Neuronal messenger ribonucleoprotein transport follows an aging Lévy walk *Nat. Commun.* **9** 344

[24] Huda S *et al* 2018 Lévy-like movement patterns of metastatic cancer cells revealed in microfabricated systems and implicated *in vivo Nat. Commun.* **9** 4539

[25] Rhodes T and Turvey M T 2007 Human memory retrieval as Lévy foraging *Physica* A **385** 255

[26] Kello C T, Brown G D A, Ferrer-i-Cancho R, Holden J G, Linkenkaer-Hansen K, Rhodes T and Van Orden G C 2010 Scaling laws in cognitive sciences *Trends Cogn. Sci.* **14** 223

[27] Klafter J, Shlesinger M F and Zumofen G 1996 Beyond Brownian motion *Phys. Today* **49** 33

[28] Zaslavsky G M 2008 *Hamiltonian Chaos and Fractional Dynamics* (Oxford: Oxford University Press)

[29] Solomon T H, Weeks E R and Swinney H L 1993 Observation of anomalous diffusion and Lévy flights in a two-dimensional rotating flow *Phys. Rev. Lett.* **71** 3975

[30] Barkai E, Fleurov V and Klafter J 2000 One-dimensional stochastic Lévy–Lorentz gas *Phys. Rev.* E **61** 1164

[31] Margolin G and Barkai E 2005 Nonergodicity of blinking nanocrystals and other Lévy-walk processes *Phys. Rev. Lett.* **94** 080601

[32] Abe M S 2020 Functional advantages of Lévy walks emerging near a critical point *Proc. Natl Acad. Sci. USA* **117** 24336

[33] Zaburdaev V, Denisov S and Klafter J 2015 Lévy walks *Rev. Mod. Phys.* **87** 483

[34] Evans M R, Majumdar S N and Schehr G 2020 Stochastic resetting and applications *J. Phys. A: Math. Theor.* **53** 193001

[35] Evans M R and Majumdar S N 2011 Diffusion with stochastic resetting *Phys. Rev. Lett.* **106** 160601

[36] Evans M R, Majumdar S N and Mallick K 2013 Optimal diffusive search: nonequilibrium resetting versus equilibrium dynamics *J. Phys. A: Math. Theor.* **46** 185001

[37] Monthus C 2021 Large deviations for Markov processes with stochastic resetting: analysis via the empirical density and flows or via excursions between resets *J. Stat. Mech.* 033201

[38] Wang W, Cherstvy A, Kantz H, Metzler R and Sokolov I 2021 Time averaging and emerging nonergodicity upon resetting of fractional Brownian motion and heterogeneous diffusion processes *Phys. Rev.* E **104** 024105

[39] Stojkoski V, Jolakoski P, Pal A, Sandev T, Kocarev L and Metzler R 2021 Income inequality and mobility in geometric Brownian motion with stochastic resetting: theoretical results and empirical evidence of non-ergodicity *Philosophical Transactions of the Royal Society* A https://doi.org/10.1098/rsta.2021.0157

[40] Lapeyre G J and Dentz M 2017 Reaction–diffusion with stochastic decay rates *Phys. Chem. Chem. Phys.* **19** 18863

[41] Roldan E, Lisica A, Sanchez-Taltavull D and Grill S W 2016 Stochastic resetting in backtrack recovery by RNA polymerases *Phys. Rev.* E **93** 062411

[42] Reuveni S, Urbakh M and Klafter J 2014 Role of substrate unbinding in Michaelis–Menten enzymatic reactions *Proc. Natl Acad. Sci.* **111** 4391

[43] Berezhkovskii A M, Szabo A, Rotbart T, Urbakh M and Kolomeisky A B 2017 Dependence of the enzymatic velocity on the substrate dissociation rate *J. Phys. Chem.* B **121** 3437

[44] Robin T, Hadany L and Urbakh M 2019 Random search with resetting as a strategy for optimal pollination *Phys. Rev.* E **99** 052119

[45] Steiger D S, Rønnow T F and Troyer M 2015 Heavy tails in the distribution of time to solution for classical and quantum annealing *Phys. Rev. Lett.* **115** 230501

[46] Maurer S M and Huberman B A 2001 Restart strategies and internet congestion *J. Econ. Dyn. Control* **25** 641

[47] Dahlenburg M, Chechkin A V, Schumer R and Metzler R 2021 Stochastic resetting by a random amplitude *Phys. Rev.* E **103** 052123

[48] Tal-Friedman O, Pal A, Sekhon A, Reuveni S and Roichman Y 2020 Experimental realization of diffusion with stochastic resetting *J. Phys. Chem. Lett.* **11** 7350

[49] Xu P, Zhou T, Metzler R and Deng W 2020 Lévy walk dynamics in an external harmonic potential *Phys. Rev.* E **101** 062127

[50] Xu P and Deng W 2018 Fractional compound Poisson processes with multiple internal states *Math. Model. Nat. Phenom.* **13** 10

[51] Xu P and Deng W 2018 Lévy walk with multiple internal states *J. Stat. Phys.* **173** 1598

[52] Jespersen S, Metzler R and Fogedby H C 1999 Lévy flights in external force fields: Langevin and fractional Fokker–Planck equations and their solutions *Phys. Rev.* E **59** 2736

[53] Chechkin A, Gonchar V, Klafter J, Metzler R and Tanatarov L 2002 Stationary states of non-linear oscillators driven by Lévy noise *Chem. Phys.* **284** 233

[54] Chechkin A V, Klafter J, Gonchar V Y, Metzler R and Tanatarov L V 2003 Bifurcation, bimodality, and finite variance in confined Lévy flights *Phys. Rev.* E **67** 010102(R)

[55] Chechkin A V, Gonchar V Y, Klafter J, Metzler R and Tanatarov L V 2004 Lévy flights in a steep potential well *J. Stat. Phys.* **115** 1505

[56] Dybiec B, Gudowska-Nowak E, Barkai E and Dubkov A A 2017 Lévy flights versus Lévy walks in bounded domains *Phys. Rev.* E **95** 052102

[57] Dybiec B, Sokolov I M and Chechkin A V 2010 Stationary states in single-well potentials under symmetric Lévy noises *J. Stat. Mech.* P07008

[58] Zhou T, Xu P and Deng W 2020 Continuous-time random walks and Lévy walks with stochastic resetting *Phys. Rev. Res.* **2** 013103

[59] Klafter J, Blumen A and Shlesinger M F 1987 Stochastic pathway to anomalous diffusion *Phys. Rev.* A **35** 3081

[60] Klafter J and Zumofen G 1994 Lévy statistics in a Hamiltonian system *Phys. Rev.* E **49** 4873

[61] Froemberg D and Barkai E 2013 Time-averaged Einstein relation and fluctuating diffusivities for the Lévy walk *Phys. Rev.* E **87** 030104(R)

[62] Godec A and Metzler R 2013 Finite-time effects and ultraweak ergodicity breaking in superdiffusive dynamics *Phys. Rev. Lett.* **110** 020603

[63] Redner S 2001 *A Guide to First Passage Processes* (Cambridge: Cambridge University Press)

[64] Metzler R, Oshanin G and Redner S 2014 *First-Passage Phenomena and Their Applications* (Singapore: World Scientific)

[65] Chechkin A V, Metzler R, Gonchar V Y, Klafter J and Tanatarov L V 2003 First passage and arrival time densities for Lévy flights and the failure of the method of images *J. Phys. A: Math. Gen.* **36** L537

[66] Koren T, Lomholt M A, Chechkin A V, Klafter J and Metzler R 2007 Leapover lengths and first passage time statistics for Lévy flights *Phys. Rev. Lett.* **99** 160602

[67] Padash A, Chechkin A V, Dybiec B, Pavlyukevich I, Shokri B and Metzler R 2019 First-passage properties of asymmetric Lévy flights *J. Phys. A: Math. Theor.* **52** 454004

[68] Padash A, Chechkin A V, Dybiec B, Magdziarz M, Shokri B and Metzler R 2020 First passage time moments of asymmetric Lévy flights *J. Phys. A: Math. Theor.* **53** 275002

[69] Palyulin V V, Chechkin A V, Klages R and Metzler R 2016 Search reliability and search efficiency of combined Lévy–Brownian motion: long relocations mingled with thorough local exploration *J. Phys. A: Math. Theor.* **49** 394002

[70] Palyulin V V, Mantsevich V N, Klages R, Metzler V R and Chechkin A V 2017 Comparison of pure and combined search strategies for single and multiple targets *Eur. Phys. J.* B **90** 170

[71] Palyulin V V, Blackburn G, Lomholt M A, Watkins N W, Metzler R, Klages R and Chechkin A V 2019 First passage and first hitting times of Lévy flights and Lévy walks *New J. Phys.* **21** 103028

[72] Zhou T, Xu P and Deng W 2021 Gaussian process and Lévy walk under stochastic non-instantaneous resetting and stochastic rest *Phys. Rev.* **104** 054124

[73] Capała K, Padash A, Chechkin A V, Shokri B, Metzler R and Dybiec B 2020 Lévy noise-driven escape from arctangent potential wells *Chaos* **30** 123103

[74] Guggenberger T, Chechkin A and Metzler R 2021 Fractional Brownian motion in superharmonic potentials and non-Boltzmann stationary distributions *J. Phys. A: Math. Theor.* **54** 29LT01

[75] Xu P, Deng W and Sandev T 2020 Lévy walk with parameter dependent velocity: Hermite polynomial approach and numerical simulation *J. Phys. A: Math. Theor.* **53** 115002

[76] Prudnikov A P, Brychkov Y A and Marichev O I 1990 *Integrals and Series* (London: Gordon and Breach)